Analysis of the $\tilde{A}\ ^1A_2 \leftarrow \tilde{X}\ ^1A_1$ and $\tilde{a}\ ^3A_2 \leftarrow \tilde{X}\ ^1A_1$ Electronic Transitions in Selenocarbonyl Difluoride

by

Mehmet Yaman Bölük, B.Sc.

A Thesis

submitted to the Department of Chemistry

in partial fulfillment of the requirements

for the degree of

Master of Science

June 1982

Brock University

St. Catharines, Ontario

ABSTRACT

The absorption spectrum of F_2CSe in the 18800-21900 cm^{-1} region has been recorded at -77°C and 22°C under the conditions of medium resolution. The responsible electronic promotion is $\pi^* \leftarrow n$ excitation which leads to $^3A_2$ and $^1A_2$ excited states. Progressions in ν_1', ν_2', ν_3', ν_4' and ν_4'' have been identified in the spectrum and have been analyzed in terms of vibronic transitions between a planar ground state and a nonplanar excited state. The origins of the $\tilde{a}\ ^3A_2 \leftarrow \tilde{X}\ ^1A_1$ and $\tilde{A}\ ^1A_2 \leftarrow \tilde{X}\ ^1A_1$ systems were assigned to the bands at 19018 cm^{-1} and 19689 cm^{-1}. This has given a singlet-triplet splitting $^1A_2 - {}^3A_2$ pf 671 cm^{-1}. The out-of-plane wagging levels were found to be anharmonic. Barrier heights of 2483 cm^{-1} and 2923 cm^{-1} were obtained for the $^1A_2$ and $^3A_2$ upper states from a fitting of the energy levels of a Lorentzian-quadratic function to the observed levels in the out-of-plane wagging modes. For the $^1A_2$ and $^3A_2$ states nonplanar equilibrium angles of 30.1° and 31.4° have been evaluated respectively.

ACKNOWLEDGMENTS

The author would like to express his gratitude to Professor D. C. Moule for the constant guidance, encouragement and continuous cooperation in the entire work of the project.

He would like to thank Dr. A. Haas of the Ruhr Universität, West Germany, who kindly provided the $(SeCF_2)_x$ compound.

He also wishes to acknowledge the glassblower, J. Vandenhoff, for the construction of the special design vacuum line, and S. Judge for the skillful typing of the thesis.

The awards of Teaching Assistantship and Research Fellowship from the National Research Council are gratefully acknowledged.

TABLE OF CONTENTS

LIST OF TABLES

LIST OF FIGURES

CHAPTER 1

INTRODUCTION

The electronic structures of molecules containing chromophores such as the carbonyl and thiocarbonyl groups have been the subject of extensive research, much of which has been devoted to the studies of the electronic spectra of these molecules. While techniques such as inelastic electron scattering and photoelectron spectroscopy have been employed for this purpose, most of the information about the electronic states has come from optical absorption or emission spectroscopy.

The simplest of the carbonyl or thiocarbonyl molecules are the tetra-atomic XYC = Z where X and Y are hydrogen, chlorine, bromine, and fluorine, and Z is oxygen or sulfur. In general, the complexity of the optical spectrum increases exponentially with the number of atoms in the system. For example, the number of degrees of freedom for a nonlinear polyatomic molecule is 3N-6 where N is the number of atoms. For this class of molecules vibrational motions can be resolved into the six normal modes of motion. As each vibrational level acts as an origin for the addition of levels from the other five molecular vibrations, the density of states increases rapidly with the vibrational quantum numbers and with the number of atoms in the molecule. What is rather surprising is that the vibrational assignment for the prototype system H_2CO had to be completely revised in the last year. ν_3' has been established to lie at 1293.05 cm^{-1}.[1]

The spectroscopy of the carbonyl and thiocarbonyl compounds in the visible and near-ultraviolet region is of importance to the area of photochemistry and photophysics. The photochemistry of molecules containing these chromophores requires a knowledge of the quantum numbers of the transitions of the bands or lines involved in the absorption process. This

information must precede any discussion of the photochemistry or photophysics and it becomes one of the motivating forces for the study of the electronic spectrum of molecules of this type.

Spectroscopists view the molecules in higher electronic states in the same way in which the chemists view the molecules in the stable ground state. That is, the dynamical structure of molecules in the excited electronic states are no more or less important than the structure in the ground electronic state. The ground electronic state which is given the label $\tilde{X}$ has a rigid planar structure for these molecules. This means that the $X_2C = Z$ species belong to the C_{2v} symmetry while the mixed halide molecules XYC = Z belong to the C_s point group. The excited states of these molecules however are nonplanar to varying degrees and the two groups of molecules then undergo a loss of symmetry to the C_s and C_1 respectively. It is the reduction of the symmetry and creation of a nonplanar excited state which are of considerable interest in the carbonyl and thiocarbonyl class of molecules.

In 1953 Walsh[2] constructed a set of orbital energy diagrams from semi-empirical theory in which the energy of the one electron orbitals was correlated against the distortion or bending of the bonds within the molecule. In the case of formaldehyde Walsh correlated the energy levels as a function of the non-planar distortion of the molecule. The correlation was taken between the planar (180^o) configuration and the right angle pyramidal (90^o) configuration. His analysis showed that all of the orbitals became less bonding except the π^* orbital with out-of-plane distortion. Within three years Brand[3] was able to verify this result in his pioneering study on the $\pi^* \leftarrow n$ transition which lies at 3500 $\mathring{A}$.

Since that time the literature[4] on the first systems of formaldehyde have grown rapidly. Also the accessibility of the spectrum and its open

appearance has made H_2CO the standard spectrum for testing new techniques. For these reasons and because H_2CO has a molecular prototype carbonyl series, it has and will receive the most attention of any tetraatomic molecule.

The other carbonyl and thiocarbonyl C_s and C_{2v} symmetry halides have been analyzed. Often the analysis has been done with the view to characterizing the differences between the carbonyl halide and the H_2CO molecular prototype. These studies have shown that the pyramidal-like structure of the excited state is very sensitive to the nature of the attached groups. The analysis of the near-ultraviolet spectra of the series: H_2CO[5,6,7], HFCO[8], F_2CO[9,10], Cl_2CO[11], H_2CS[12,13,14], F_2CS[15], Cl_2CS[16,17], ClFCS[18] was fitted into a common pattern. Fluorine has the effect of increasing the barrier height over that of hydrogen. The barrier height to molecular inversion in the first singlet excited state labelled as $\tilde{A}$ for F_2CO[10] is 8200 cm^{-1} while in H_2CO[19] it is 316 cm^{-1}. Similar trends have been observed in the thiocarbonyl series of molecules with the 3076 cm^{-1} barrier height in F_2CS[15] falling to 0 cm^{-1} in H_2CS[20]. Other changes also occur on halogen substitution. These are somewhat smaller and more difficult to elucidate.

At this time there is no literature on the electronic spectroscopy of selenocarbonyl compounds. This is partly because tetraatomic selenocarbonyl compounds are unstable and their toxicity is unknown. It is believed, though, that they should be handled with caution. The F_2CSe species has recently been reported in the literature and the spectrum of F_2CO and F_2CS are known and relatively well understood. We felt that the study of F_2CSe would allow spectrocorrelations to be carried out between the carbonyl, thiocarbonyl and selenocarbonyl series of molecules.

Some spectral information is available for the lower $\tilde{X}$ state of F_2CSe. Matrix IR of F_2CSe, and gas phase[21], and liquid phase Raman spectra[22] have been

studied. All of the six ground state fundamental frequencies have been identified and the spectral bands were assigned. The structural information has come from an electron diffraction study.[23] The structure by this method is given in Figure 1. The more accurate microwave study has not been made.

FIGURE 1

The Geometry of F_2CSe in its Two Lowest States

(a) Structure of the Ground Electronic State[23]

(b) Structure of the First Excited State

$r_{CSe} = 1.743$ Å

$r_{CF} = 1.314$ Å

$\beta = 107.5^{o}$

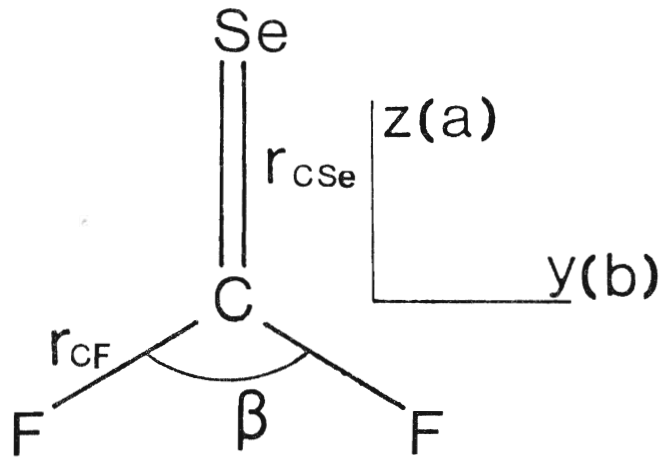

-a-

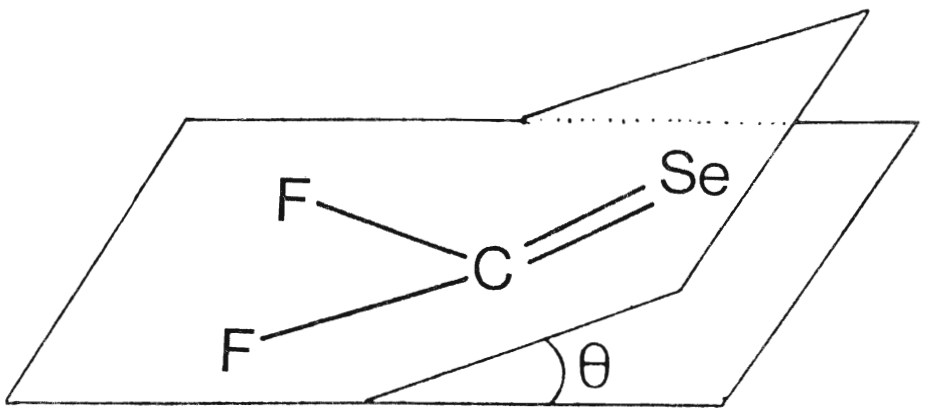

-b-

CHAPTER 2

ELECTRONIC STATES OF THE F_2CSE MOLECULE

2.1 The Electronic Structure

The usual method for constructing the MO's of a molecule is the linear combinations of AO's (LCAO). Each atom in the molecular system is considered to contribute at least one atomic orbital to the set of MO's. Thus each MO is written as

$$\psi_i = \sum_j c_{ij} \phi_j \tag{2.1}$$

in which ψ_i is the wave function for the ith MO and ϕ_j is the jth AO.

The MO's form a basis for the irreducible representations of the molecular point group. Since the planar ground state configuration of F_2CSe, like H_2CO, is classified under the C_{2v} molecular point group, each molecular orbital is a basis for one of the irreducible representations listed in Table 1. Figure 1(a) shows the coordinate axis system and the geometry of F_2CSe in the ground state.

The inner shells and valence AO's of carbon, selenium and fluorine atoms are chosen for a minimal-basis set MO treatment. Linear combinations of these 38 basis AO's give a LCAO approximation to the 38 lowest MO's of F_2CSe. As a preliminary step in finding the MO's of a molecule, it is helpful to construct linear combinations of the original basis AO's such that each linear combination transforms according to one of the molecular symmetry species. Such linear combinations of F_2CSe which are called symmetry orbitals are summarized in Table 2. Each MO is a linear combination of those group orbitals having the same symmetry species as the MO.

There is no ab-initio calculation about the orbital energies and the coefficients of the symmetry orbitals in the literature. The energy ordering

TABLE 1

C_{2v} Character Table

	E	$C_2(Z)$	$\sigma_v(XZ)$	$\sigma_v'(YZ)$		
A_1	1	1	1	1	T_Z	
A_2	1	1	-1	-1		R_Z
B_1	1	-1	1	-1	T_X	R_Y
B_2	1	-1	-1	1	T_Y	R_X

TABLE 2

Symmetry Orbitals of F_2CSe

Symmetry Species	Carbon	Selenium	Fluorine
a_1	C(1s)	Se(1s)	$F_1(1s) + F_2(1s)$
	C(2s)	Se(2s)	$F_1(2s) + F_2(2s)$
	$C(2p_z)$	$Se(2p_z)$	$F_1(2p_y) + F_2(2p_y)$
			$F_1(2p_z) + F_2(2p_z)$
		Se(3s)	
		$Se(3p_z)$	
		$Se(3d_{z2})$	
		$Se(3d_{x2-y2})$	
		Se(4s)	
		$Se(4p_z)$	
		$Se(4d_{z2})$	
		$Se(4d_{x2-y2})$	
a_2		$Se(3d_{xy})$	$F_1(2p_x) - F_2(2p_x)$
		$Se(4d_{xy})$	
b_1	$C(2p_x)$	$Se(2p_x)$	$F_1(2p_x) + F_2(2p_x)$
		$Se(3p_x)$	
		$Se(3d_{xz})$	
		$Se(4p_x)$	
		$Se(4d_{xz})$	
b_2	$C(2p_y)$	$Se(2p_y)$	$F_1(1s) - F_2(1s)$
		$Se(3p_y)$	$F_1(2s) - F_2(2s)$
		$Se(3d_{yz})$	$F_1(2p_y) - F_2(2p_y)$
		$Se(4p_y)$	$F_1(2p_z) - F_2(2p_z)$
		$Se(4d_{yz})$	

of the three highest occupied and one unoccupied orbitals of F_2CSe can be estimated qualitatively by the theoretical calculations which have been given for F_2CO[24], H_2CO[25], and H_2CS[26,27].

The estimated electronic configuration of the ground state of F_2CSe is

$$(\text{inner shell electrons})(a_1:\sigma_{CSe})^2(b_1:\pi_{CSe})^2(b_2:n_{ySe})^2 \quad {}^1A_1$$

The three highest occupied molecular orbitals are σ_{CSe}, π_{CSe}, and n_{ySe} orbitals having a_1, b_1 and b_2 symmetry, respectively. The symmetry species of the electronic wave function for a molecular state can be obtained by taking the direct product of the irreducible representations to which each of these one electron symmetry MO's belong. Therefore the overall symmetry of the ground state of the F_2CSe molecule is A_1.

The first unoccupied orbital is an antibonding π^*_{CSe} orbital, having b_1 symmetry. The lowest electronic excited state occurs when one of the electrons in the $(b_2:n_{ySe})$ nonbonding orbital is excited into the antibonding $(b_1:\pi^*_{CSe})$ orbital. The electronic configuration is then

$$(\text{inner shell electrons})(a_1:\sigma_{CSe})^2(b_1:\pi_{CSe})^2(b_2:n_{ySe})^1(b_1:\pi^*_{CSe})^1$$

Since the two different orbitals (b_2) and (b_1) each contain a single electron, the excited electronic configuration gives states with total spin S = 0 and S = 1. Because the product of the two functions of species b_2 and b_1, transform as a_2, $^3A_2$ and $^1A_2$ states are obtained. According to Hund's rule the triplet state $^3A_2$ has lower energy than the singlet state $^1A_2$. The electronic transition from the $^1A_1$ ground state to the $^3A_2$ and $^1A_2$ excited states will be considered in Chapter 3.

The electronic configuration of the other excited states and their symmetries are shown in Table 3.

TABLE 3

The Electronic States and Symmetries of F_2CSe

Electronic Configuration	State Symmetry
(filled subshells)$(a_1:\sigma_{CSe})^2(b_1:\pi_{CSe})^2(b_2:n_{ySe})^2$	A_1
(filled subshells)$(a_1:\sigma_{CSe})^2(b_1:\pi_{CSe})^2(b_2:n_{ySe})^1(b_1:\pi^*_{CSe})^1$	$b_2 \times b_1 = A_2$
(filled subshells)$(a_1:\sigma_{CSe})^2(b_1:\pi_{CSe})^1(b_2:n_{ySe})^2(b_1:\pi^*_{CSe})^1$	$b_1 \times b_1 = A_1$
(filled subshells)$(a_1:\sigma_{CSe})^2(b_1:\pi_{CSe})^1(b_2:n_{ySe})^2(a_1:\sigma^*_{CSe})^1$	$b_1 \times a_1 = B_1$
(filled subshells)$(a_1:\sigma_{CSe})^2(b_1:\pi_{CSe})^2(b_2:n_{ySe})^1(a_1:\sigma^*_{CSe})^1$	$b_2 \times a_1 = B_2$
(filled subshells)$(a_1:\sigma_{CSe})^1(b_1:\pi_{CSe})^2(b_2:n_{ySe})^2(b_1:\pi^*_{CSe})^1$	$a_1 \times b_1 = B_1$

2.2 Variation of the Molecular Orbital Energies with Geoemtry

The molecular orbitals of the valence electrons of F_2CSe have similarities to those of H_2CO. Hence a correlation of the formaldehyde orbitals can be made with those of F_2CSe between the planar C_{2v} and pyramidal C_s configurations (Figure 1(a), (b)). Walsh's[2] primary postulate on which his diagram (Figure 2) is based is that a molecular orbital has a lower energy if, on changing the bond angle at the atomic center, the MO changes from being a p-type orbital to being built from an s-type AO. The $a_1(\sigma_{CH})$, $b_2(\sigma_{CH})$ and $a_1(\sigma_{CO})$ bonding orbitals all decrease in binding energy on bending the molecule since at a 90^o angle these become pure carbon p-type orbitals, while at 120^o the carbon orbitals are sp^2. The $b_1(\pi_{CO})$ orbital, formed by the overlap of $p_x(O)$ and $p_x(C)$, is less binding in the bent molecule. The oxygen lone pair orbital $b_2(n_yO)$ is only slightly influenced by bending, inasmuch as it interacts with the $b_2(\sigma_{CH})$ orbital. The $b_1(\pi^*_{CO})$ is antibonding in C_{2v} and nonbonding in C_s. The effect of bending is to mix the carbon 2s orbital into the $2p_x$ carbon orbital and, finally at 90^o the orbital is 2s nonbonding. The $a_1(\sigma^*_{CO})$ orbital is destabilized by the bending because of the introduction of more p character as was the case with the σ bonding orbitals. The ground state electronic structure of formaldehyde is obtained by adding 12 electrons into the six most strongly binding orbitals so the molecule is planar. From Figure 2, nonplanar excited $\tilde{A}\ ^1A_2$, $\tilde{a}\ ^3A_2$, $\tilde{B}\ ^1A_1$, and $\tilde{b}\ ^3A_1$ states can be predicted.

Similarly a slight increase in energy with an increase in the out-of-plane angle is expected for all molecular orbitals of F_2CSe up to and including the nonbonding orbital. However, a marked decrease in energy on correlation to the a' molecular orbital of the nonplanar configuration is expected for the $b_2(\pi^*_{CSe})$ MO. Thus F_2CSe, in its $\tilde{A}\ ^1A_2$, $\tilde{a}\ ^3A_2$, $\tilde{B}\ ^1A_1$ and $\tilde{b}\ ^3A_1$ states, is expected to be bent out-of-plane.

FIGURE 2

Walsh Diagram for Formaldehyde

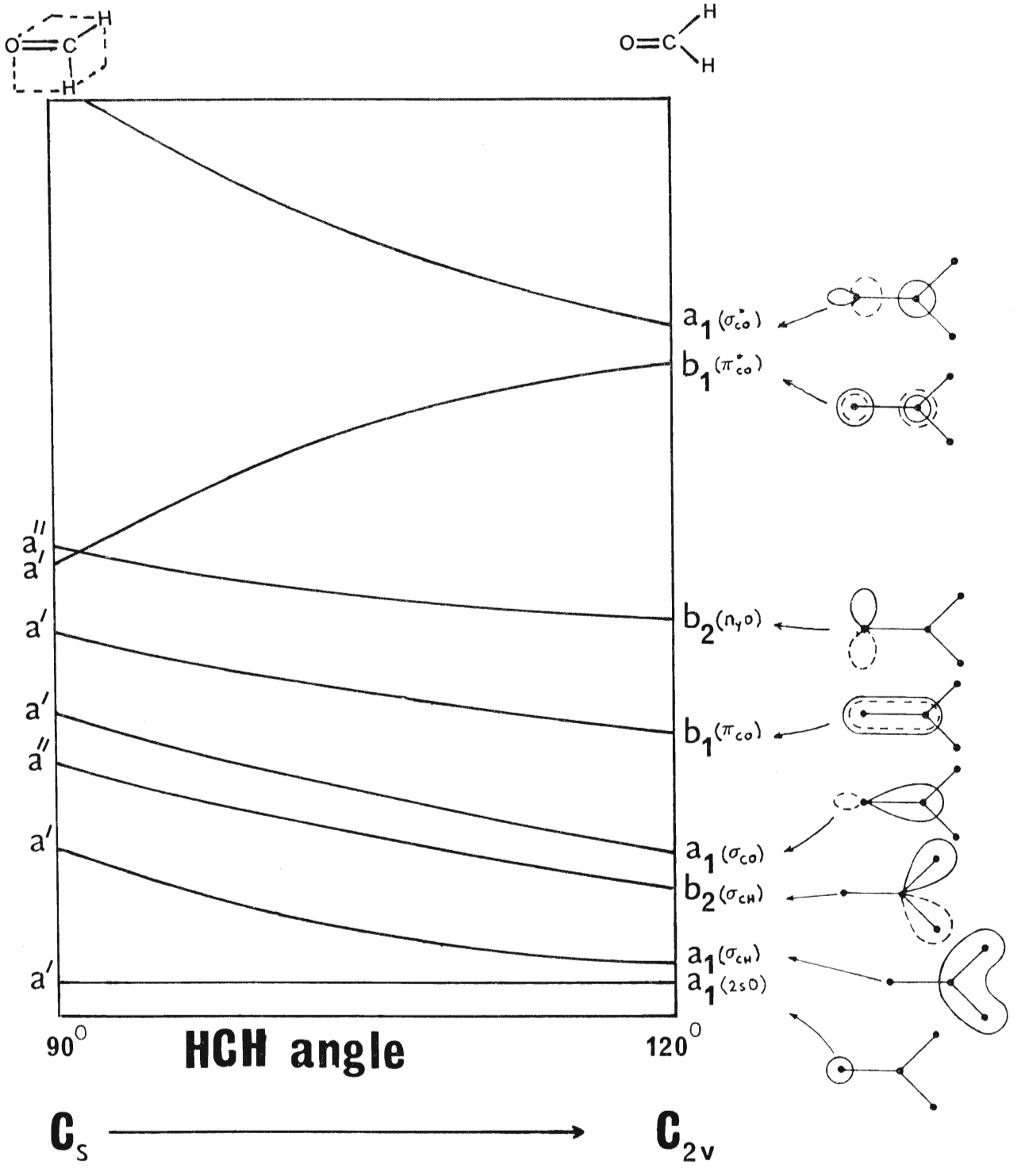
a1 (σ*co)
b1 (π*co)
a″
a′
b2 (n,o)
a′
b1 (πco)
a′
a″
a1 (σco)
a′
b2 (σCH)
a1 (σCH)
a′
a1 (2sO)
90°
HCH angle
120°
Cs
C2v

2.3 Molecular Vibrations of the Ground State $\tilde{X}\ ^1A_1$

F_2CSe, like its oxygen and sulfur analogs, belongs to the C_{2v} point group in the ground state and has six normal modes of vibration. Three of these transform as a_1, two as b_2, and the last one transforms as b_1 species under the operation of the C_{2v} point group. The infrared spectrum of F_2CSe has been studied and the frequencies of the normal modes assigned by Haas and his coworkers[21,22] (Table 4).

The normal modes are functions of a set of internal displacement vectors. Six internal parameters can be used to describe the structure of the F_2CSe molecule: r_1 and r_2, r_3, β, α_1 and α_2, these being the instantaneous values of the two C—F and C═Se bond lengths, $\widehat{FCF}$, and the two $\widehat{FCSe}$ bond angles. Instead of $(\alpha_1 + \alpha_2)$, one can equivalently specify an instantaneous bending angle θ made by the C═Se bond and the projection of the bisector of FCF plane. Displacements of the internal coordinates from the equilibrium position are shown as Δr_1, Δr_2, Δr_3, $\Delta\beta$, $\Delta\alpha_1$ and $\Delta\alpha_2$.

The six genuine internal vibrations span the irreducible representations $3A_1 + B_1 + 2B_2$.[28] Symmetry adapted linear combinations (SALC) of the internal coordinates and normalization give the six internal symmetry coordinates:

type A_1

$S_1 = \Delta r_3$ — C═Se stretching

$S_2 = \frac{1}{\sqrt{2}}(\Delta r_1 + \Delta r_2)$ — Symmetric CF stretching

$S_3 = \Delta\beta$ — In plane $\widehat{FCF}$ bending

type B_1

$S_4 = \Delta\theta$ — Out-of-plane bending

type B_2

$S_5 = \frac{1}{\sqrt{2}}(\Delta r_1 - \Delta r_2)$ — Antisymmetric CF stretching

$S_6 = \frac{1}{\sqrt{2}}(\Delta\alpha_1 - \Delta\alpha_2)$ — Antisymmetric $\widehat{FCSe}$ bending

TABLE 4

Ground State Fundamental Frequencies of F_2CSe[21,22] (cm^{-1})

a_1	ν_1	1287
	ν_2	705
	ν_3	432
b_1	ν_4	575
b_2	ν_5	1207
	ν_6	351

The contributions of the bond stretching and the angle bending to the normal modes according to their symmetry types are known for the F_2CO[29] and F_2CS[30] molecules. Comparison of the frequencies of the normal modes and force constants can be made between F_2CO, F_2CS and F_2CSe which are given in Table 5. Consider the modes ν_2 and ν_5. In the series $F_2CO/F_2CS/F_2CSe$ ν_2 takes the values 962/789.3/705 whereas ν_5 shows little variation, 1208/1200/1207. The reduction in ν_2 can be explained by a mixing of the S_1 and S_2 internal coordinates. While it is permissible to use the labels ν_1(C═X) and ν_2(CF) in F_2CO and F_2CS, it is necessary here to use the notation ν_1(C═X + CF) and ν_2(C═X + CF). ν_3 involves $\widehat{FCF}$ bending, ν_4 the out-of-plane bending and ν_5, ν_6, respectively, the antisymmetric CF stretching and $\widehat{FCSe}$ bending coordinates. Figure 3 gives a representation of the normal modes.[31]

2.4 Molecular Vibrations of the Excited States $\tilde{A}\ ^1A_2$ and $\tilde{a}\ ^3A_2$

The $^{1,3}A_2$ excited states of F_2CSe are expected to be nonplanar and have two energetically equivalent equilibrium pyramidal configurations. The two configurations of the inverting molecule are separated by a potential barrier which hinders interconversion of the two forms.

Figure 4 shows the evolution of the potential energy diagram as a central barrier is introduced. The effect of an inversion barrier on the vibrational levels of a nonplanar molecule can be analyzed, using the harmonic oscillator wave functions as a basis set. In the absence of a perturbing potential, the harmonic oscillator energy levels are equally spaced. V is the harmonic oscillator quantum number. As a barrier is introduced at the bottom of the potential well, the vibrational energy levels draw together in pairs and the two lowest levels are displaced the most. In the case of an infinitely high barrier the pairs of levels coalesce, and no inversion doubling

TABLE 5

Force Constants and Fundamental Frequencies

of F_2CO, F_2CS and F_2CSe

	F_2CO[29]	F_2CS[30]	F_2CSe[21,22]
ν_1	1880.5 (CO)	1365.2 (CS)	1287 (CSe + CF)[a]
ν_2	962 (CF)	789,3 (CF)	705 (CSe + CF)
ν_3	581 (FCF)	526.2 (FCF)	432 (FCF)
ν_4	743.2 (out-of-plane)	623.2 (out-of-plane)	575 (out-of-plane)
ν_5	1208 (CF anti)	1200 (CF anti)	1207 (CF anti)
ν_6	619.9 (FCO anti)	418 (FCS anti)	351 (FCSe anti)
f_{CO}	14.818[29]	-	-
f_{CS}	-	6.625[32]	-
f_{CSe}	-	-	5.096[21]
f_{CF}	6.734[29]	6.541[32]	6.536[21]

[a] S_1 and S_2 are believed to be strongly coupled in the formation of Q_1 and Q_2.

FIGURE 3

Normal Vibrations of the Planar F_2CSe Molecule

(The displacement vectors are not drawn on scale.)

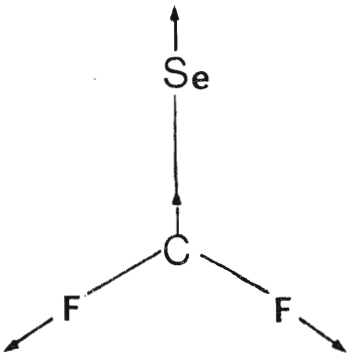

$\nu_1(a_1)$

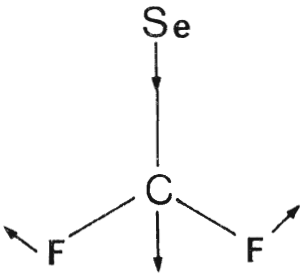

$\nu_2(a_1)$

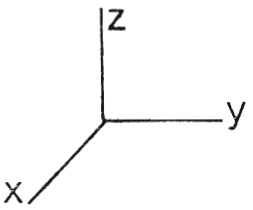

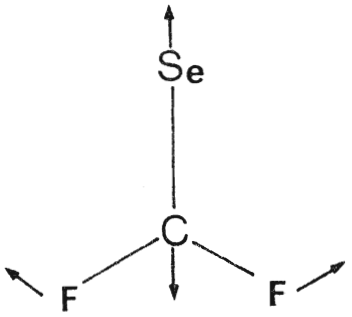

$\nu_3(a_1)$

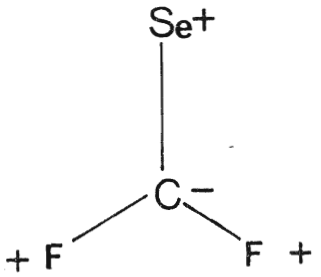

$\nu_4(b_1)$

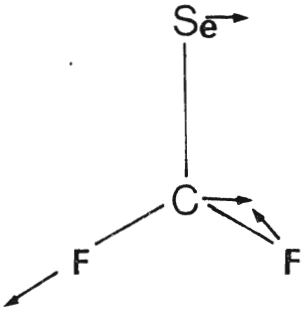

$\nu_5(b_2)$

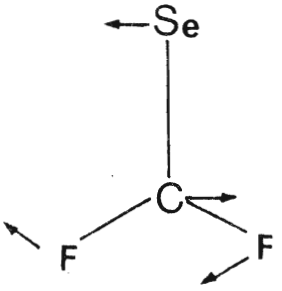

$\nu_6(b_2)$

FIGURE 4

Potential Energy, V(Q), vs Out-of-plane Coordinate, Q, for

(a) Rigid Planar Molecule

(b) Nonrigid Nonplanar Molecule

(c) Rigid Nonplanar Molecule

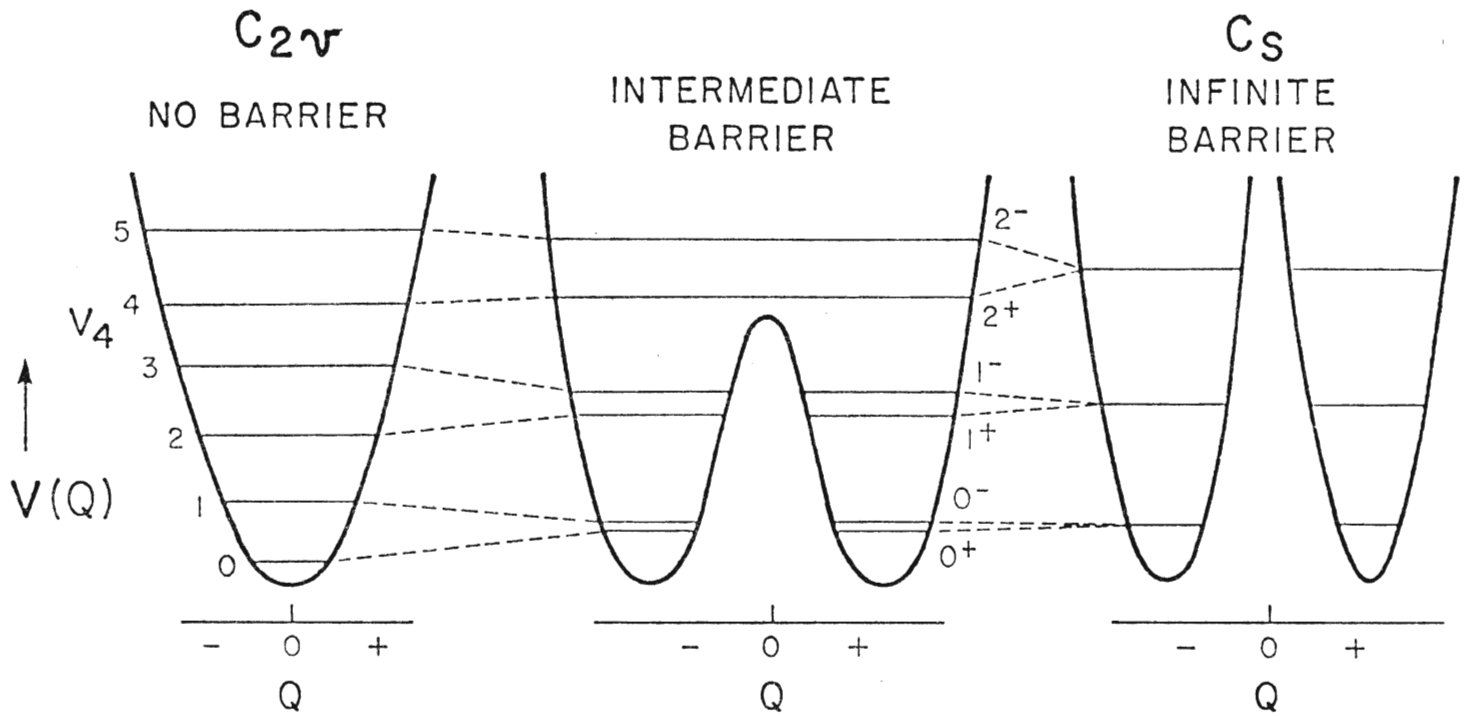
C2v
NO BARRIER
INTERMEDIATE BARRIER
Cs
INFINITE BARRIER
V4
V(Q)
5
4
3
2
1
0
2⁻
2⁺
1⁻
1⁺
0⁻
0⁺
- 0 +
Q
- 0 +
Q
- 0 +
Q

-a- -b- -c-

is apparent. Classically, the molecule is isolated in one of the two identical potential wells, and its vibrational levels are doubly degenerate. This is true for nonplanar molecules whose potential energy barriers are much larger than the energies of the lower vibrational levels.

Let the harmonic oscillator function represent the potential function for the out-of-plane bending motion, $\nu_4(b_1)$ of a planar molecule and assume a small amplitude of vibration. With a planar equilibrium structure, two equivalent configurations are obtained by inverting the molecule. The eigenfunctions of the energy levels are characterized by their symmetry. They are alternately symmetric and antisymmetric with respect to inversion. The symmetric levels are designated by (+) and the antisymmetric levels by (-). If the equilibrium structure becomes nonplanar, the symmetric and antisymmetric levels draw together, and each pair of vibrational levels consists of (+) and (-) components. The lowest vibrational level of a molecule is always symmetric and the upper member is antisymmetric. Alternatively, each vibrational level for a high inversion barrier may be thought of as two inversion sublevels: one is symmetric and the other is antisymmetric to inversion.

For a high barrier, the lower vibrational levels lie below the top of the potential barrier. The two minima in the potential function represents the two energetically equivalent equilibrium forms of the inverting molecule. When the molecule resides in a vibrational state below the top of the barrier, it is classically impossible for it to invert to its other form. This would restrict inversion to molecules in the vibrational states above the top of the barrier. However, the quantum mechanical tunnelling effect allows molecules to tunnel through the barrier at a rate which is a function of the height and width of the barrier. The molecule is not associated with either potential minimum but is "distributed" across both minima in Figure 4. If ψ_L and ψ_R are

eigenfunctions describing the molecule in the left and right minima of Figure 4(b) the wave functions for the double minima oscillator are:

$$\psi_V^{\pm} = \frac{1}{\sqrt{2}} \left[\psi_L \pm \psi_R \right] \tag{2.2}$$

ψ_V^+ is symmetric, ψ_V^- antisymmetric for inversion.

The time-dependent wave function is:

$$\psi_V(t) = \frac{1}{\sqrt{2}} \left[\psi_V^+ + \psi_V^- e^{2\pi i \nu t} \right] e^{2\pi i E_V^+ t/h} \tag{2.3}$$

$\psi_V(t)$ indicates that the tunnelling process is continuous in nature. E_V^+ is the energy of the V^+ state and $h\nu$ is the energy difference between the two inversion states. $\psi(t)$ gives a measure of the rate of tunnelling in terms of the energy separation of the two inversion levels.

ψ_V^+ belongs to the A_1 representation and ψ_V^- to the B_1 representation. The symmetric and antisymmetric combination functions in Equation (2.2) are exactly degenerate when the pyramid is rigid (i.e. has an infinite barrier for inversion). For any finite barrier the degeneracy is split and for planar molecules with a harmonic restoring force the familiar equidistant vibrational levels are nondegenerate.

CHAPTER 3

VIBRONIC TRANSITIONS OF F_2CSe

3.1 The Electric Dipole Allowed Transitions

The probability that an oscillating electromagnetic field induces a transition from vibronic states e"v" to e'v' per unit time and per unit radiation energy is given by[33]

$$W(e'v'e''v'') = \frac{8\pi^3}{3h^2} \left|M(e'v'e''v'')\right|^2 \tag{3.1}$$

where W(e'v'e"v") is the Einstein probability coefficient and M(e'v'e"v") is the transition moment integral. The transition moment integral can be written

$$M(e'v'e''v'') = \langle \psi_{e'v'} \left| P \right| \psi_{e''v''} \rangle \tag{3.2}$$

where P, the electric dipole operator, can be separated into a component, P_e, due to the electrons and a component, P_N, due to the nuclei

$$P = P_e(r) + P_N(Q) \tag{3.3}$$

where r and Q are, respectively, the electronic and nuclear coordinates. The nuclear coordinates are best expressed in terms of the normal coordinates.

$\psi_{e''v''}$ and $\psi_{e'v'}$ are, respectively, the vibronic wave functions of the ground and excited states. The Born-Oppenheimer approximation states that the nuclear motion is sufficiently slow with respect to the electronic motion that the molecular wave function ψ_{ev} for the vth vibrational level of the eth electronic state can be reduced to the product of an electronic and vibrational wave function.

$$\psi_{ev} = \psi_e(r,Q)\psi_v(Q) \tag{3.4}$$

The transition integral takes the form

$$M(e'v'e''v'') = \langle\psi_{e'}(r,Q)|P_e(r)|\psi_{e''}(r,Q)\rangle\langle\psi_{v'}(Q)|\psi_{v''}(Q)\rangle + \langle\psi_{v'}(Q)|P_N(Q)|\psi_{v''}(Q)\rangle\langle\psi_{e'}(r,Q)|\psi_{e''}(r,Q)\rangle \quad (3.5)$$

As the electronic wave functions are orthogonal, the transition moment then becomes

$$M(e'v'e''v'') = \langle\psi_{e'}(r,Q)|P_e(r)|\psi_{e''}(r,Q)\rangle\langle\psi_{v'}(Q)|\psi_{v''}(Q)\rangle \quad (3.6)$$

The dipole components will transform as the translation operators of the molecular point group which are $A_1(z)$, $B_1(x)$, and $B_2(y)$ in C_{2v} symmetry. If the direct product of $\Gamma(e') \times \Gamma(e'')$ does not contain $\Gamma(P_e)$, then the matrix element $\langle\psi_{e'}(r,Q)|P_e(r)|\psi_{e''}(r,Q)\rangle$ is vanishing. For $\pi^* \leftarrow n$ transition in C_{2v} symmetry $\Gamma(e') \times \Gamma(e'')$ transforms as A_2. This gives allowed magnetic dipole but not electric dipole transitions. The transition to the $n\pi^*$ state is spatially forbidden for electric dipole radiation. On the other hand, electric dipole transitions are allowed between the ground and the $A_1(\pi\pi^*)$ states.

3.2 Vibrational-Electronic Interactions

Equation (3.6) is derived on the assumption that the Born-Oppenheimer approximation holds, so that the vibronic wave function can be factored as $\psi_e\psi_v$. ψ_e is the eigenfunction of the electronic Hamiltonian

$$H_e\psi_e = E_e\psi_e \quad (3.7)$$

To the exact electronic Hamiltonian operator for the system of electrons in the field of the fixed nuclei is now added a perturbation, which represents the variations of total electronic energy with small nuclear displacements.[34,35] The Hamiltonian may be expanded in powers of the normal coordinates. The linear term in displacement Q_V is taken to be the perturbation H':

$$H' = \sum_{V=1}^{3N-6} (\partial H/\partial Q_V)_0 Q_V$$

$$= \sum_V V_V Q_V \tag{3.8}$$

The term $\partial H/\partial Q_V$ is evaluated at the equilibrium position Q_0 of the Vth normal mode. The electronic wave function of the perturbed Hamiltonian is written as an expansion of the zeroth order wave function. For simplicity it is assumed that only the upper state ψ_e' is perturbed. If ψ_m^0 is the zeroth order approximation to the particular excited state ψ_e', and ψ_n^0 are the zeroth order wave functions for the other electronic states, then the first order correction to ψ_e' is written as

$$\psi_e'(r,Q) = \psi_m^{(0)}(r,Q_0) + \sum_{n\neq m} \sum_V \frac{Q_V \langle \psi_m^{(0)} | V_V | \psi_n^{(0)} \rangle}{E_n^{(0)} - E_m^{(0)}} \psi_n^{(0)}(r,Q_0)$$

$$= \psi_m^{(0)}(r,Q_0) + \sum_{n\neq m} \sum_V Q_V C_{nm}^{(V)} \psi_n^{(0)}(r,Q_0) \tag{3.9}$$

where

$$C_{nm}^{(V)} = \frac{\langle \psi_m^{(0)} | V_V | \psi_n^{(0)} \rangle}{E_n^{(0)} - E_m^{(0)}} \tag{3.10}$$

The transition moment integral of Equation (3.2) now takes the form

$$M(e'v'e''v'') = \langle \psi_m^{(0)}(r,Q_0) | P_e | \psi_e''(r,Q_0) \rangle \langle \psi_{v'}(Q) | \psi_{v''}(Q) \rangle +$$

$$\sum_{n\neq m} C_{nm}^{(v')} \langle \psi_n^{(0)}(r,Q_0) | P_e | \psi_e''(r,Q_0) \rangle \langle \psi_{v'}(Q) | Q_{v'} | \psi_{v''}(Q) \rangle \tag{3.11}$$

As it was shown earlier, the first part of Equation (3.11) vanishes because of symmetry for the $^1A_2 \leftarrow {}^1A_1$ transition of F_2CSe. The $^1A_2 \leftarrow {}^1A_1$ bands are the result of the second part of Equation (3.11). For nonvanishing $M(e'v'e''v'')$ at least one of the $\langle \psi_n^{(0)}(r,Q_0) | P_e | \psi_e''(r,Q_0) \rangle$ and the coefficient

$C_{nm}^{(v')}$ within the summation term must be nonzero. V_v transforms as the vibrational normal coordinates. For nonzero $C_{nm}^{(v')}$ the irreducible representation of $\psi_n^{(0)}$, V_v and $\psi_m^{(0)}$ must contain the totally symmetric representation. These conditions may be satisfied by an interaction of the A_2 electronic state with a_2, b_2 and b_1 vibrational modes. These couplings cause respectively mixing of the $^1A_2(n\pi^*)$ state with the $^1A_1(\pi\pi^*)$, $^1B_1(\sigma\pi^*)$ and $^1B_2(n\sigma^*)$ states.

The admixture of $^1B_2(n\sigma^*)$ character, through the b_1 vibration, with the $^1A_2$ state is held responsible for the B polarized vibronic transitions, while $^1B_1(\sigma\pi^*)$ character (admixed through b_2 vibrations) is invoked to account for C polarized vibronic transitions in the spectrum. The A polarized vibronic transitions result from the admixture of the $^1A_1(\pi\pi^*)$ character through combinations of b_1 and b_2 vibrations. The expected polarizations of the bands in the $^1A_2 \leftarrow {}^1A_1$ transition for odd or even quanta changes of the three species of normal modes are summarized in Tables 6 and 7.

3.3 Spin-Orbit Interactions

According to the spin selection rule, $\Delta S = 0$, the $\tilde{a}\ ^3A_2 \leftarrow \tilde{X}\ ^1A_1$ transition is forbidden for electric dipole radiation, if the electronic wave function can be separated into a spin and a space-dependent part. A coupling of the magnetic field due to the orbital motion of the electron and the spin magnetic moment of the electron, however, is capable of breaking down the space-spin factorization. If a triplet state $\tilde{T}$ is perturbed by a singlet state $\tilde{S}$, then according to McClure[36], M(e'v'e"v") for the transition $\tilde{T} \leftarrow \tilde{X}$, where $\tilde{X}$(e"v") is the ground state, is given by

$$M(e'v'e''v'') = \sum_S \frac{\langle\psi_T(r,Q)|H_{SO}|\psi_S(r,Q)\rangle}{(E_S - E_T)}\langle\psi_S(r,Q)|P_e|\psi_{e''}(r,Q)\rangle$$

$$\langle\psi_{v'}(Q)|\psi_{v''}(Q)\rangle \qquad (3.12)$$

TABLE 6

Vibrational-Electronic Couplings that Allow $\tilde{A}\ ^1A_2 \leftarrow \tilde{X}\ ^1A_1$ Transition

$\nu_1' + \nu_2' + \nu_3'$	ν_4'	$\nu_5' + \nu_6'$	Vibrational Symmetry of Excited State $\Gamma(v')$	Electronic Symmetry of Excited State $\Gamma(e')$	Vibronic Symmetry $\Gamma(e')x\Gamma(v')=\Gamma(e'v')$	Electronic Symmetry of Ground State $\Gamma(e'')$	Symmetry of Induced Moment $\Gamma(e'')x\Gamma(e'v')=\Gamma(P_e)$	Band Type
Unrestricted	Even	Even	$a_1 \times a_1 \times a_1 = a_1$	A_2	$A_2 \times a_1 = A_2$	A_1	-	Electric Dipole Forbidden
Unrestricted	Even	Odd	$a_1 \times a_1 \times b_2 = b_2$	A_2	$A_2 \times b_2 = B_1$	A_1	B_1	X(C)
Unrestricted	Odd	Even	$a_1 \times b_1 \times a_1 = b_1$	A_2	$A_2 \times b_1 = B_2$	A_1	B_2	Y(B)
Unrestricted	Odd	Odd	$a_1 \times b_1 \times b_2 = a_2$	A_2	$A_2 \times a_2 = A_1$	A_1	A_1	Z(A)

TABLE 7

Pathways for the Vibrational-Electronic Coupling of the $\tilde{A}\ ^1A_2$ State to the Higher Intravalence States

Ground State $\Gamma(e'')$	Excited State $\Gamma(e')$	Species of V_v $\Gamma(V_v)$	Perturbing State $\Gamma(m)$	Induced Moment $\Gamma(e'') \times \Gamma(m) = \Gamma(P_e)$	Band Type
A_1	A_2	A_1	-	-	Electric Dipole Forbidden
A_1	A_2	A_2	$A_1(\pi\pi^*)$	A_1	Z(A)
A_1	A_2	B_1	$B_2(n\sigma^*)$	B_2	Y(B)
A_1	A_2	B_2	$B_1(\sigma\pi^*)$	B_2	X(C)

Such a perturbation will not occur unless the spin-orbit operator, H_{SO}, gives the first integrand the transformation properties of the totally symmetric A_1 species. Since the components of the orbital part of H_{SO} transform under the operations of the C_{2v} group as rotations about the x, y or z axes, the components may be classified respectively as B_2, B_1 or A_2. $\psi_{\tilde{T}}$ transforms as A_2, and hence the perturbing singlet $\tilde{S}$ in the first integrand may be either $^1B_1$, $^1B_2$ or $^1A_1$ according to the R_x, R_y or R_z transformation properties of H_{SO} (Table 8).

3.4 The Oscillator Strength

Mulliken has transformed the Einstein absorption coefficients into a measure of intensity, the oscillator strength f, which is given by:[33]

$$f = \frac{16\pi^2 mc}{3h^2e^2}\,\sigma\left|M(e'v'e''v'')\right|^2 \tag{3.13}$$

and f is related to the absolute intensity by[37]

$$f = 4.319 \times 10^{-9}\,\frac{1}{bc}\int_{\sigma_1}^{\sigma_2} A_\sigma d\sigma \tag{3.14}$$

where m is the mass of the electron, c is the concentration, b is the path length, and σ_1 and σ_2 are, respectively, the lower and higher wavenumber limits of the electronic absorption band under consideration. The absorbance (A_σ) is a function of the wave number.

Transitions that are both electronically and spin-allowed characteristically have an oscillator strength of about 0.01-0.4 while values ranging from 10^{-6} to 10^{-4} are expected for vibronically allowed or spin forbidden transitions.

TABLE 8

Pathways for the Spin-Orbit Coupling of the $\tilde{a}\ ^3A_2$ State

to the Higher Intravalence States

Ground State $\Gamma(e'')$	Excited State $\Gamma(e')$	Component of H_{SO}	Species of H_{SO} $\Gamma(H_{SO})$	Perturbing Singlet State $\Gamma(s)$	Induced Moment $\Gamma(P_e)$	Band Type
A_1	A_2	H(X)	B_2	$B_1(\sigma\pi^*)$	B_1	X(C)
A_1	A_2	H(Y)	B_1	$B_2(n\sigma^*)$	B_2	Y(B)
A_1	A_2	H(Z)	A_2	$A_1(\pi\pi^*)$	A_1	Z(A)

CHAPTER 4

EXPERIMENTAL

4.1 Preparation of the F_2CSe Compound

Selenium compounds are potentially dangerous. Special precautions were needed in preparing monomeric F_2CSe. A vacuum rack was mounted on a sheet of plywood which would fit into the fumehood. This was portable and allowed the construction and the testing of the vacuum line to be done on the laboratory bench.

The vacuum line was of grease-free construction. High vacuum teflon stopcocks and ground glass joints with Viton O-rings were used. The system was pumped to 0.01 torr vacuum by a single stage mechanical vacuum pump. The vacuum was checked by an Edwards thermocouple gauge. Gas pressures were measured by a silicon oil closed end manometer. The fused quartz absorption cell was connected directly to the vacuum line.

F_2CSe was prepared by the pyrolysis of $(SeCF_2)_x$ at 200°C in a vacuum. The starting material $(SeCF_2)_x$, which was analytically pure, was donated by Dr. A. Haas. The set up of the vacuum line is given in Figure 5. Polymeric sample was inserted into the bulb (A). Solid polymer was cracked and vaporized in a vacuum by the application of heat from a heat gun. The pyrolysis was carried out in the spiral pyrex tube (B) which contains 20 turns. The total length of the pyrolysis tube was 250 cm, and the diameter was 0.6 cm. The temperature of the pyrolysis tube was 200°C which was maintained by the tube furnace (C). The temperature was controlled by a large variac and measured by a copper-constanton thermocouple. The pyrolysis reaction was:

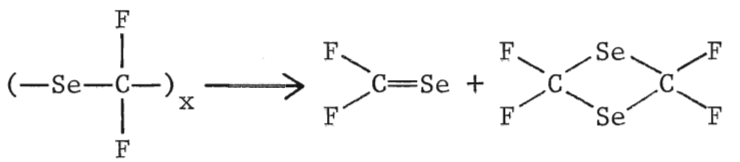

FIGURE 5

Experimental Set-Up for the Preparation of the F_2CSe Monomer

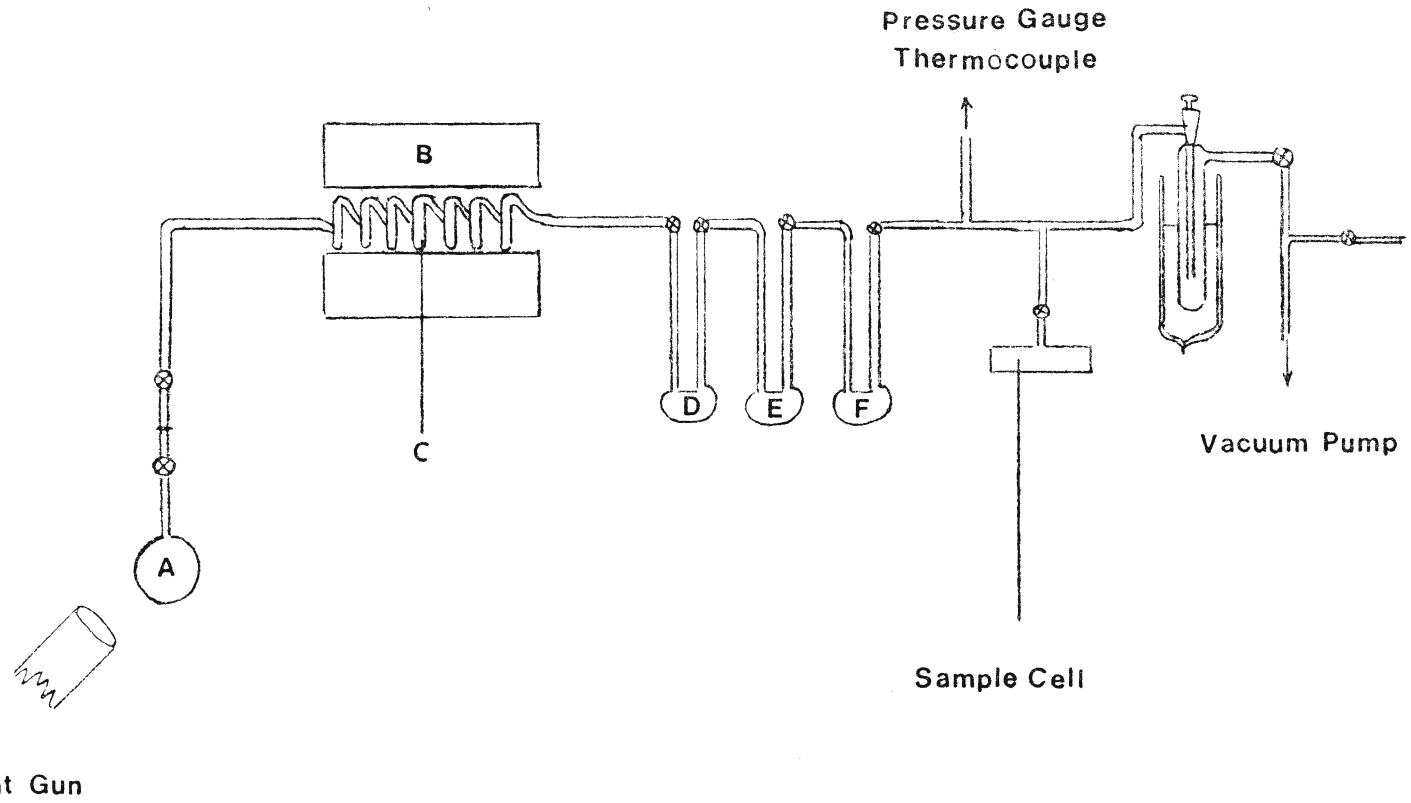
Pressure Gauge
Thermocouple
B
C
D
E
F
A
Vacuum Pump
Sample Cell
Heat Gun

Besides selenocarbonyl difluoride, the cyclic dimer 2,2,4,4-tetrafluoro-1,3-diselenetane was obtained.

The monomer and the cyclic dimer were passed through the traps (D), (E) and (F). Trap (D) was surrounded by a slurry of solid CO_2 and acetone giving a temperature of $-78^{o}C$. Trap (E) was immersed in a toluene slush bath at $-95^{o}C$ and the last trap (F) was cooled to liquid nitrogen temperature, $-193^{o}C$. The cyclic dimer was trapped in (D), monomer in trap (E), while (F) removed the highly volatile materials.

The material in trap (E) is believed to be monomeric F_2CSe with trace impurities of the cyclic dimer. In the visible and UV region, the monomer and cyclic dimer give rise to very different spectra. For example the monomer is expected to display low energy $\pi^* \leftarrow n$ and $\pi^* \leftarrow \pi$ absorptions whereas the first transition in the dimer would be a $3s \leftarrow n$ Rydberg transition. Due to the potential toxicity, the experiments were carried out over a period of four days.

4.2 Recording of the Spectra

Survey spectra of F_2CSe were recorded over the 6000-2000 Å region with a Cary-Model 14 spectrophotometer with 1 torr and 22 torr cell pressures. The structured bands of the lower transition were clearly observed with 22 torr pressure in a 10 cm cell. These bands were centered at 4400 Å. A pressure of only 1 torr was required to give an appreciable absorption in this region. This system was too diffuse for high resolution studies.

Medium resolution spectra of the lower region were photographed with a 6 meter Ebert Spectrograph[38] at a reciprocal linear dispersion of 0.65 Å/mm. A slit width of 30 μ was employed. The path length of the cell was 90 cm. At room temperature 70 and 12 torr pressures were used which are equivalent to 8.28×10^{-2} and 1.42×10^{-2} m-atms. pressure x pathlength respectively. Spectra were also recorded at dry ice temperatures at 6.0×10^{-3} m-atm.

A 450 watt Xenon arc lamp was used as a continuous source of radiation. Lines from a Fe-Ne hollow cathode discharge lamp were used for the calibration of the spectra. Spectra were recorded on Ilford FP4 film and developed in Kodak Dektol developer.

4.3 Measurement and Calibration of the Spectra

Spectra were enlarged 2.5 times on Kodabromide F5 paper and mounted on sheets of bristol board. A Precision Tool Instrument travelling microscope was used to measure the Fe-Ne hollow cathode emission lines. The wave lengths of the calibration lines were taken from a list compiled by H. M. Croswhite.[39] The vacuum wavelengths and wave numbers of the standard iron emission lines and the calibrated absorption bands were displayed on the top and the bottom of each print.

Profiles of the absorption bands were obtained from the negatives with a single beam microdensitometer (Herzberg Institute of Astrophysics).

CHAPTER 5

ASSIGNMENT OF THE SPECTRA AND THE RESULTS

5.1 Survey Spectra of the F_2CSe System

Three absorption bands appeared in the UV-visible region. These bands can be classified by their intensity, frequency and also by their structure.

The first absorption occurred in the visible region, and is shown in Figure 6 as an extensive band from about 5000 Å to 3500 Å. It consists of a broad band which has a maximum at about 4400 Å (22727 cm^{-1}), (2.818 ev), and possesses a complicated vibrational fine structure. The maximum molar extinction coefficient (ε_{max}) is 25.0 L $mole^{-1}cm^{-1}$ and the oscillator strength for this system is 3.5×10^{-4}. This was obtained from Equation 3.14.

At higher energies a second system was observed which is completely free from vibrational structure, and is illustrated in Figure 7. The center of this band was measured to be 2400 Å (41677 cm^{-1}), (5.167 ev). This is a strong system which has ε_{max} = 1047.9 lt $mole^{-1}cm^{-1}$ and $f = 2.47 \times 10^{-2}$.

The oscillator strength values were calculated from the observed gas pressure in the cell. It was assumed that the sample was pure, and that the cyclic dimer did not introduce a measurable partial pressure. The oscillator strengths reported here represent the lower limits to the true experimental values.

The final system was observed as the onset of an absorption at about 2000 Å. The center of the system was not observed in these experiments. The high absorption strength would lead us to believe that the transition has a high oscillator strength.

5.2 Assignments of the Electronic Transitions

The low energy absorption λ_{max} = 4400 Å, $f = 3.5 \times 10^{-4}$ has the

FIGURE 6

The Visible Spectrum of F_2CSe Recorded with a Cary Model 14 Spectrophotometer. The pressure of the gas was 22 mmHg, the path length was 10 cm.

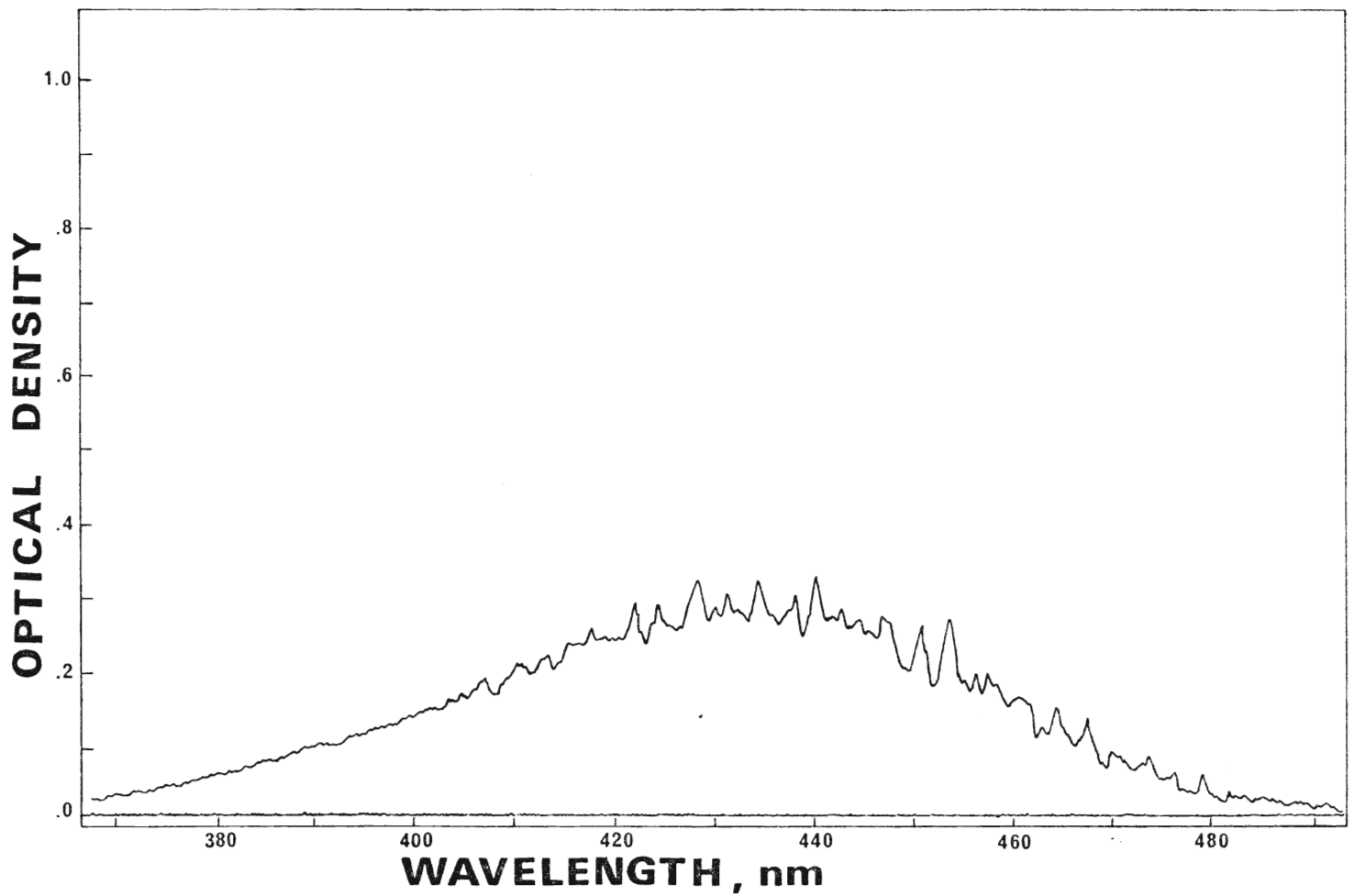
OPTICAL DENSITY
1.0
.8
.6
.4
.2
.0
380
400
420
440
460
480
WAVELENGTH, nm

FIGURE 7

The Near-Ultraviolet Spectrum of F_2CSe Recorded with a Cary Model 14 Spectrophotometer. The pressure of the gas was 1 mmHg, the path length was 10 cm.

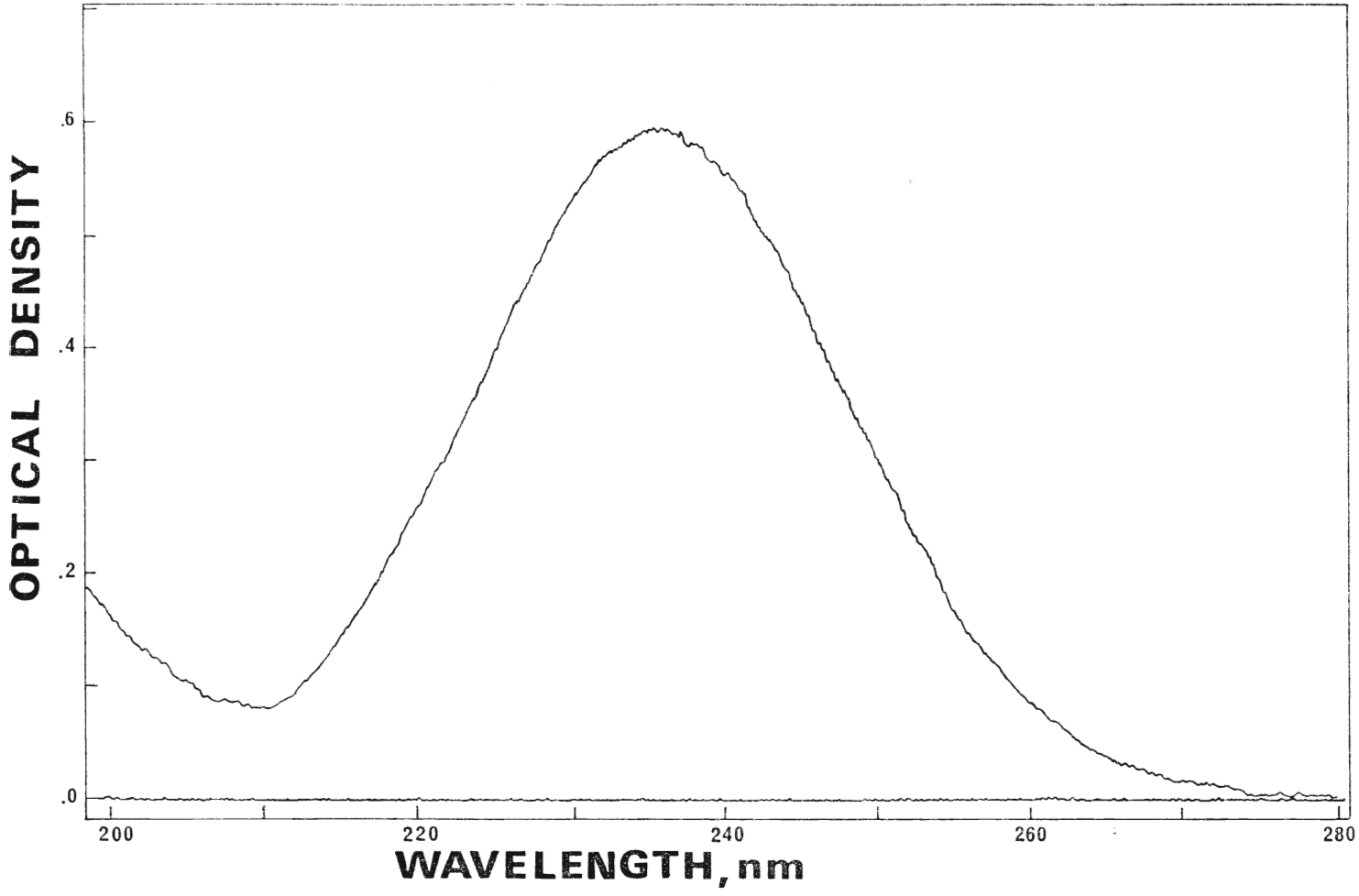
OPTICAL DENSITY
.6
.4
.2
.0
200
220
240
260
280
WAVELENGTH, nm

characteristics of a transition which is not allowed by electric dipole selection rules. The ground state, with filled electronic shells, has A_1 symmetry. Since T_x, T_y and T_z transform as B_1, B_2 and A_1 respectively, then the spatially forbidden transition must terminate on the remaining representation, A_2. Therefore, the first observed absorption in the spectrum is assigned to the spin forbidden and spin allowed $\tilde{a}\ ^3A_2 \leftarrow \tilde{X}\ ^1A_1$ and $\tilde{A}\ ^1A_2 \leftarrow \tilde{X}\ ^1A_1$ transitions respectively. The singlet and triplet $^1A_2$ and $^3A_2$ excited states arise from the promotion of an electron from the nonbonding orbital on the selenium to the antibonding π^* orbital which is located in the selenocarbonyl bond. This assignment is totally compatible with the thiocarbonyl and carbonyl counterparts. The observed vibrational fine structure also supports the $\pi^* \leftarrow n$ assignment as will be discussed in a later section.

The assignment of the second system does not create any difficulty at this stage of analysis. It has very high oscillator strength which is an indication of an allowed electronic transition. While the bands in this region of the spectrum are not found in the carbonyl-containing species, the thiocarbonyl analogs show very similar absorptions. The assignment of the bands in the thiocarbonyl molecules are now well established. The electron promotion and electronic transitions to a spin allowed and orbitally allowed (z polarized) $\tilde{B}\ ^1A_1 \leftarrow \tilde{X}\ ^1A_1$ transition. This is the assignment which is given to the λ_{max} = 2400 Å band which is shown in Figure 7.

Our assignment of the third system is more tentative. While MO calculations are not available for this molecule, a simple-minded picture would place the 3s ← n electron promotion as the third transition in the spectrum. The existing experimental data are unable to make this assignment more certain.

5.3 Vibrational Analysis of the $\tilde{a}\ ^3A_2 \leftarrow \tilde{X}\ ^1A_1$ Electronic Transition

The starting point for the vibrational analysis of the lower electronic

transition was a recognition of two major factors.

The first of these relates to the higher atomic number of selenium z = 34 compared to sulfur and oxygen which have atomic numbers 16 and 8 respectively. The higher electron density in this molecule is expected to relax the $\Delta S = 0$ spin selection rule, with the result that the singlet-triplet transition is expected to contribute to the intensity of the low energy end of the spectrum.

The other major assumption which was used in the initial assignment is that the molecule is nonplanar in the excited singlet and triplet states. A consideration of the electron configuration and Walsh's rule lead to the conclusion that $\pi^* \leftarrow n$ and $\pi^* \leftarrow \pi$ states have stable pyramidal structures. The spectrum therefore would display the characteristics of inversion doubling.

Moreover the combination of a planar ground state and a nonplanar excited state should give rise to very strong activity in the ν_4' progressions. The progressions in ν_4'' would occur in the spectrum with the same intensity except that they would be reduced by the Boltzmann thermal population factors. The ground state frequencies tabulated in Table 5 give $\nu_4'' = 575$ cm^{-1}. The Boltzmann Factor at 25^{o}C for this interval is 6.27×10^{-2}. Transitions in ν_4'' would be expected to appear weakly in the spectrum as hot bands. The comparison of the spectrum observed at room temperature with those recorded at dry ice temperatures reveal these hot bands. A search in the spectrum for intervals extending to lower frequencies in 575 cm^{-1} and terminating on temperature sensitive band yielded the intervals of Table 9. Without further analysis it is possible to conclude that the molecule in the upper state is highly nonplanar and that the barrier to inversion is large. The hot band interval, however, contains not only ν_4'' but also the inversion doubling splitting. For example, in the singlet-singlet system the interval $4_0^1 - 4_1^0$ is equal to $\nu_4'' + \Delta$ where Δ

TABLE 9

Frequency Differences Isolating ν_4'' ($\tilde{A}\ ^1A_2 \leftarrow \tilde{X}\ ^1A_1$) ($cm^{-1}$)

$\Delta\nu_4''$	Attached Difference	0	2_0^1
0 - 1	$4_0^1 - 4_1^0$	-	-
	$4_0^3 - 4_1^2$	575	-
	$4_0^5 - 4_1^4$	577	-
	$4_0^7 - 4_1^6$	601	-

TABLE 10

Frequency Differences Isolating ν_4'' ($\tilde{a}\ ^3A_2 \leftarrow \tilde{X}\ ^1A_1$) ($cm^{-1}$)

$\Delta\nu_4''$	Attached Difference	0	2_0^1
0 - 1	$0_0^0 - 4_1^1$	-	-
	$4_0^2 - 4_1^3$	575	-
	$4_0^4 - 4_1^5$	-	572
	$4_0^6 - 4_1^7$	565	-

equals $4^1 - 4^0$ which is shown in Figure 8(a). The selection rules for singlet-triplet transition for the equivalent intervals $0_0^0 - 4_1^1$ is equal to $\nu_4'' - \Delta$ which is given in Figure 8(b). The difference between the observed intervals and the ν_4'' from the IR data is a measure of the splittings. The data of Tables 9 and 10 show that the largest Δ observed is 26 cm^{-1}. This is a relatively small value of the inversion doubling splitting and is a direct indicator of a substantial barrier height in the excited state.

The band pattern was very complex and it appeared that many combinations of intervals would be possible. Under the moderate resolution used here, some rotational structures were evident in the bands. A successful set of frequency differences was obtained by combining the wave numbers of pairs of bands which had the similar rotational contour. An interval 540 ± 5 cm^{-1} can be found which was common to 21 frequency differences. The intervals were grouped into a smooth progression in up to five members. It is believed that these progressions play the dominant rule in forming the overall band structure. They are assigned as progressions in ν_4'.

The hot band intervals combined with the IR value of ν_4'' lead to small values and it was concluded that the barrier heights in both the $\tilde{A}\ ^1A_2$ and $\tilde{a}\ ^3A_2$ states are high. Also associated with the high barrier would be an appreciable nonplanar distortion of the equilibrium structure from its planar ground state. The transition from the ground state to the excited state converts the planar molecule into pyramidal form. Such a structural change which occurs on excitation gives rise to intense Franck-Condon activity in the vibronic bands which are assigned to the modes corresponding to the internal coordinates which best describe the molecular distortion. The out-of-plane mode is Q_4. Therefore, the bands which appear strongly in the spectrum should involve activity in ν_4. The 540 cm^{-1} frequency interval on Franck-Condon grounds therefore can

FIGURE 8

Organization of the ν_4 Progression in the Absorption Spectra of F_2CSe with C_{2v} Symmetry

(a) For the $\tilde{A}\ ^1A_2 \leftarrow \tilde{X}\ ^1A_1$ Transition

(b) For the $\tilde{a}\ ^3A_2 \leftarrow \tilde{X}\ ^1A_1$ Transition

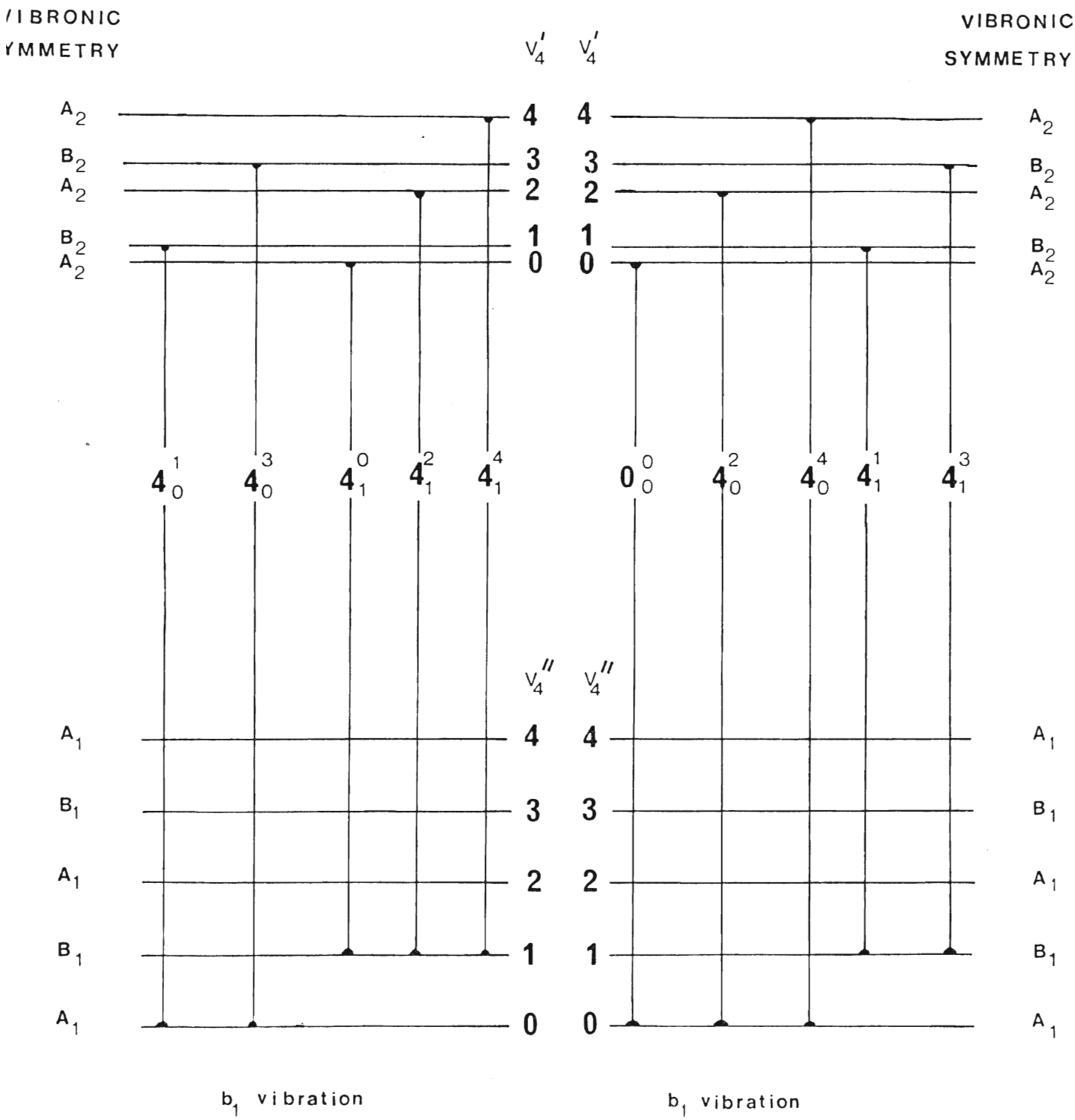
VIBRONIC SYMMETRY
V_4'
A_2
B_2
A_2
B_2
A_2
4
3
2
1
0
4_0^1
4_0^3
4_1^0
4_1^2
4_1^4
V_4''
A_1
B_1
A_1
B_1
A_1
4
3
2
1
0
b_1 vibration
- a -
VIBRONIC SYMMETRY
V_4'
A_2
B_2
A_2
B_2
A_2
4
3
2
1
0
0_0^0
4_0^2
4_0^4
4_1^1
4_1^3
V_4''
A_1
B_1
A_1
B_1
A_1
4
3
2
1
0
b_1 vibration
- b -

be assigned to quanta in ν_4.

A similar assignment can also be made by comparing the ground and excited state frequencies. In Figure 4 the potential function for Q_4 in the ground state (planar) is correlated to the potential function for the excited state (nonplanar). This diagram shows that the introduction of a small maximum (barrier) into the potential function at the origin has the effect of widening and flattening the potential well. The effect of the barrier is to reduce the force constant (k) which describes the harmonic part of the potential. If the reduced mass (μ) of the system is assumed to be the same in the two states, then the smaller force constant in the upper state has the effect of reducing the frequency. A drop in the out-of-plane mode ν_4 from 575 cm^{-1} to about 540 cm^{-1} is not unexpected. This reduction is attributed to the loss of molecular planarity on excitation.

In general, the energy levels of one mode couple to the energy levels of another mode, creating states which are combinations of the modes. The number of levels which can be found in a region of energy space therefore increases rapidly from the electronic origin of the system. The consequence of this is that while the region of the spectrum containing the origin band is relatively simple, the higher energy regions quickly become complex. The assignment of the vibrational quantum numbers to the ν_4 mode therefore began at the low energy (red) end of the spectrum. It is here that the spectrum is expected to be dominated by bands from the $\tilde{a}\ ^3A_2 \leftarrow \tilde{X}\ ^1A_1$ singlet-triplet transition. The first band that was recorded in the long path experiments was a doublet that was found at 19018 and 18990 cm^{-1}. The double headed feature of this band was found to be replicated in other regions of the spectrum. For example, the band at 19561 cm^{-1} appears in combination with a second band at 19539 cm^{-1}. Indeed the bands of the singlet-triplet transition appear as

twins throughout the spectrum. This behaviour is similar to what has been observed in the corresponding $\tilde{a}\ ^3A_2 \leftarrow \tilde{X}\ ^1A_1$ transition in the thiocarbonyl analog, F_2CS.[40] The separation between the doublet features varied from 28 cm^{-1} for the origin band to 20 cm^{-1} for the higher members of the ν_4' mode. It is believed that the two bands are rotational features in a single vibronic band. It is possible that what is observed here are heads in the S-form and Q-form branches of a single singlet-triplet transition.

The assignment of the bands in the singlet-triplet region of the spectrum has been made over the 5300 to 4700 Å range. The first band that was observed in the spectrum was assigned to the vibronically allowed transition 0_0^0 at 19018 and 18990 cm^{-1}. A clear progression of five members in a frequency interval 543 cm^{-1} was found to lock onto the 0_0^0 origin band. The frequencies for this progression are tabulated in Table 11. This progression is assigned to the out-of-plane bending motion in the upper electronic state ν_4'.

Progressions in ν_4' were followed back to the bands at 19415 cm^{-1} and 19805 cm^{-1} which were assigned to pseudo origins in this mode. The bands are found to combine with the origin band in a frequency of 397 cm^{-1}. Frequency differences for these progressions are given in Table 11. These intervals were assigned ν_3' which has a frequency of 432 cm^{-1} in the lower $\tilde{X}\ ^1A_1$ state, a drop from 432 to 397 cm^{-1}. This would be associated with a small structural change in the ν_3 mode as a result of electronic excitation.

$\pi^* \leftarrow$ n electron promotion, which leads to the $\tilde{a}\ ^3A_2 \leftarrow \tilde{X}\ ^1A_1$ and $\tilde{A}\ ^1A_2 \leftarrow \tilde{X}\ ^1A_1$ electronic transitions, places an electron in an antibonding π^* orbital. In the upper electronic state the selenocarbonyl bond contains two electrons in both σ and π bonding orbitals and one electron in the π^* antibonding orbital for a bond order of 1.5. The $\tilde{X}$ ground state however has a

TABLE 11

Frequency Differences Between the Various Vibrational Levels and 0_0^0 Level of the $\tilde{a}\ ^3A_2$ Excited State (cm^{-1})

		2_0^1	2_0^2	3_0^1	3_0^2	1_0^1	$1_0^1 3_0^1$	$1_0^1 3_0^2$	$1_0^1 2_0^1 3_0^1$	$1_0^1 2_0^1 3_0^2$
0_0^0	0	671	-	397	787	-	1527	-	2183	2579
4_0^2	543	1210	1878	935	1327	1699		2472		
4_0^4	1085	1752		1477	1873	2213				
4_0^6	1615			2016						
4_0^8	2110									

nominal bond order of 2. The electron promotion creates an instability in the selenocarbonyl bond which results in an increase in bond length and reduction in the force constant. The selenocarbonyl stretching frequency in the lower $\tilde{X}\ ^1A_1$ state has a value of 1287 cm^{-1}. It would be expected therefore that ν_1' should appear as a well characterized interval in the spectrum in a frequency of about 1000 cm^{-1}. One such interval was located in the spectrum with a frequency of 1130 cm^{-1} in combination with ν_3'. Higher intervals were not observed in the spectrum because these weaker singlet-triplet bands merge into the stronger bands of the singlet-singlet transitions. Also the vibrational analysis of selenocarbonyl difluoride in the ground state from the IR and Raman studies[21,22] show that a very strong mixing occurs between S_1 and S_2, which are the CSe and CF stretching internal coordinates. The intensity distribution which results from a pair of modes which are strongly mixed in their internal coordinates is complex and can not be predicted without a full polydimensional Franck-Condon analysis. It is possible though that vibronic activity can leak from the S_1 to the S_2 mode and that ν_2 can show an anomalous intensity distribution. ν_2 was observed as a progression in ν_4 attached to the 2_0^1 and 2_0^2 bands giving rise to a ν_2' interval of 671 cm^{-1}. The reduction in frequency on the excitation in ν_2 can be associated also with the problem of the internal coordinate mixing.

The remaining modes ν_5 and ν_6 are antisymmetric with respect to two-fold rotation and reflection in the xz plane. Bands involving quanta of antisymmetric vibrations with b_2 irreducible representations are doubly forbidden in the singlet-triplet transition. They require the addition of the vibronic-spin-orbit operator to the Hamiltonian to create intensity. As such they are 10^3 times or more weaker in intensity than the totally symmetric vibrations a_1 which are forbidden by the spin-orbit selection rule. Possibly the only way

in which these levels could be observed in the spectrum would be through sequence transitions 5_1^1 and 6_1^1. At room temperature these bands would not be expected to appear in the spectrum.

5.4 Vibrational Analysis of the $\tilde{A}\ ^1A_2 \leftarrow \tilde{X}\ ^1A_1$ Electronic Transition

The temperature effect was invaluable in the assignment of the multiplicity of the bands in the spectrum. Those bands which were temperature insensitive (cold) which could not be fitted into the pattern established for the singlet-triplet transition were initially assigned to the singlet-singlet system.

The electrons in the nonbonding n_{ySe} and antibonding π^* orbitals occupy different regions of the carbon-selenium bond; also, the orbitals are orthogonal to each other. The result is that if one electron interchanges its electron spin with respect to the other electrons, the energy of the system is not greatly affected.

The vibrational frequencies in the $\tilde{A}\ ^1A_2$ state should be fairly close to those observed in the $\tilde{a}\ ^3A_2$ state. Also the structure of the two electronic states which arises from the $\pi^* \leftarrow n$ electron promotion should be similar. That is, the vibrational intervals which occur in the singlet-singlet transition should be similar to those of the singlet-triplet transition. Moreover the progressions which contain these intervals should also be similar in the two states.

The progressions in ν_4 were easily located in the spectrum and are tabulated in Table 12. The observed frequencies for the $\tilde{A}\ ^1A_2$ state are very close to those of the $\tilde{a}\ ^3A_2$ state. For example: $\tilde{a}/\tilde{A}$, ν_1(1156)/1129), ν_2(671/662), ν_3(397/388), ν_4(543/539).

The spectrum could be followed out to 21668 cm^{-1} of vibrational excitation in the $\tilde{A}\ ^1A_2$ state. At this point the bands in the spectrum

TABLE 12

Frequency Differences Between the Various Vibrational Levels and the 4_0^1 Level of the $\tilde{A}\ ^1A_2$ Excited State (cm^{-1})

		2_0^1	2_0^2	2_0^3	3_0^1	3_0^2	1_0^1	$2_0^2 3_0^1$	$1_0^1 2_0^1 3_0^2$
4_0^1	0	662	1318	1973	-	-	1129	1704	2029
4_0^3	539	1197	1856	2511	927	1306	1668	2237	
4_0^5	1075	1728	2393	-	1461	1837			
4_0^7	1595				1979				
4_0^9	2111								

became very diffuse which made them difficult to locate and to measure. For this reason the vibrational analysis was carried out to 22200 cm^{-1}. The partial diffuseness of the bands limited the accuracy to which the centers could be measured to ±2 cm^{-1}.

The vibrational structure of the $\pi^* \leftarrow n$ electron promotion is presented in Figure 9 along with the assignments of the selected vibronic bands. The assignments which represent 75% of the bands in this region are shown in Table 13.

5.5 Potential Energy Functions for the Inversion Mode

Eight vibrational levels of the out-of-plane bending motion for both the $\tilde{A}\ ^1A_2$ and $\tilde{a}\ ^3A_2$ excited states were observed and are shown in Table 14. The energy levels occurred as doublets for this mode. The lower member of each vibrational eigenvalue is associated with a symmetric eigenfunction and the upper member with an antisymmetric eigenfunction. The vibrational potential for this out-of-plane problem can be treated as a one-dimensional function which implies that the interactions of this mode with the remaining vibrational modes can be neglected.

Several one-dimensional potential energy functions for the inversion mode are described in the literature.[41] In the current study three different functions were used to fit to the observed vibrational levels of F_3CSe in the two excited states. Our first model function was derived from a combination of a harmonic oscillator potential and a Gaussian term. This potential function has been used successfully for the inversion modes of a number of different pyramidal molecules.[42-45] At higher quantum numbers of ν_4', the calculated levels were found to be lower than the observed levels. Because the vibrations associated with the double-minimum potentials were highly anharmonic, a quartic term was added to the Gaussian perturbed harmonic oscillator to improve the fit.

FIGURE 9

(a) Spectrogram of the $\pi^* \leftarrow n$ Transition of F_2CSe

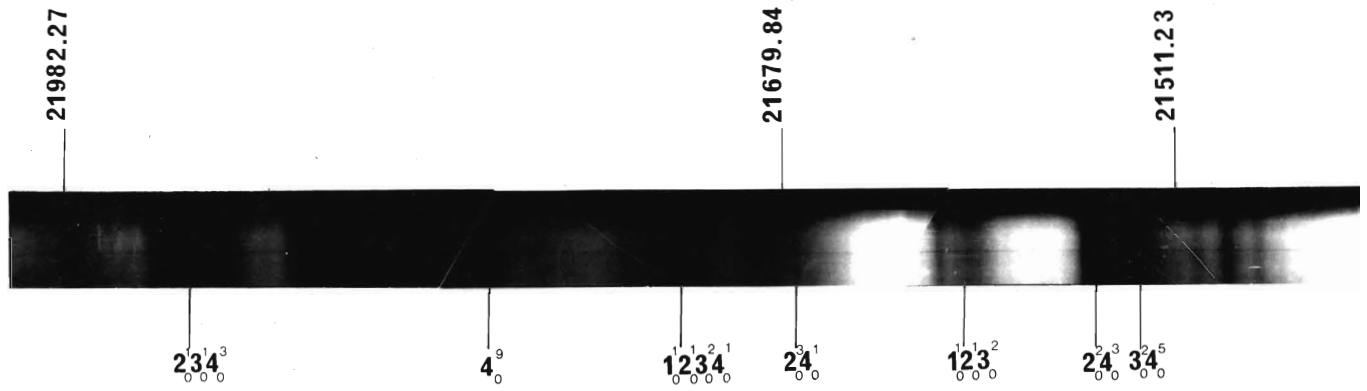
21982.27
21679.84
21511.23
$2_0^1 3_0^1 4_0^3$
4_0^9
$1_0^1 2_0^1 3_0^2 4_0^1$
$2_0^3 4_0^1$
$1_0^1 2_0^1 3_0^2$
$2_0^2 4_0^3$
$3_0^2 4_0^5$

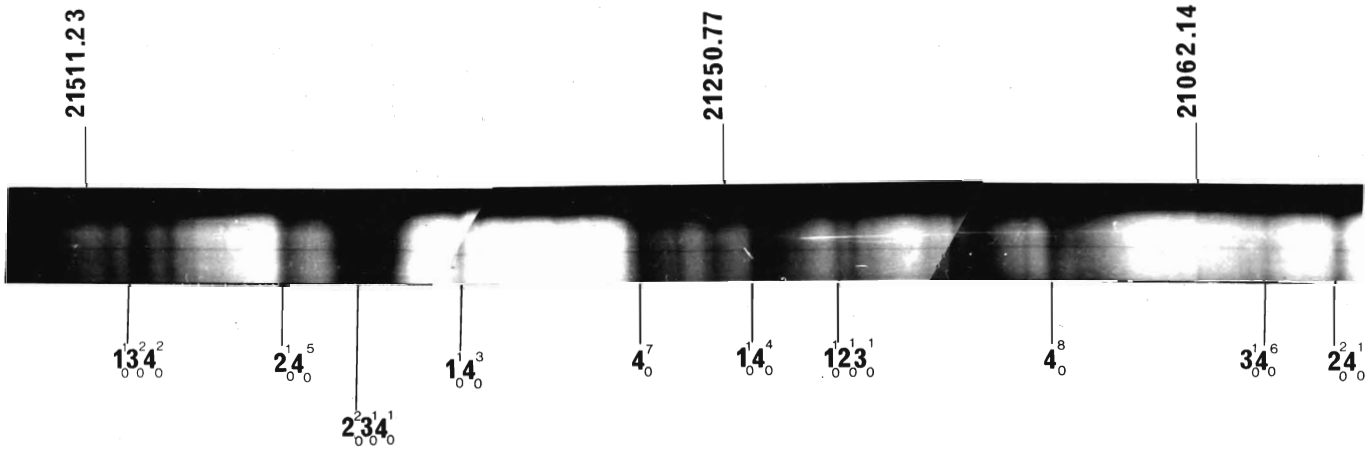
21511.23
21250.77
21062.14
$1_0^1 3_0^2 4_0^2$
$2_0^1 4_0^5$
$2_0^2 3_0^1 4_0^1$
$1_0^1 4_0^3$
4_0^7
$1_0^1 4_0^4$
$1_0^1 2_0^1 3_0^1$
4_0^8
$3_0^1 4_0^6$
$2_0^2 4_0^1$

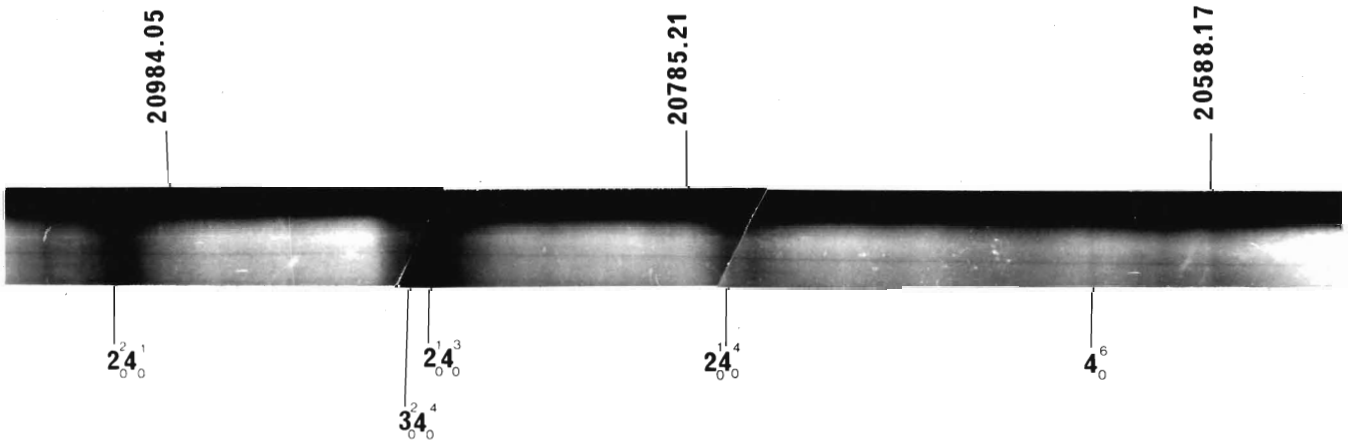
20984.05
20785.21
20588.17
$2_0^2 4_0^1$
$2_0^1 4_0^3$
$3_0^2 4_0^4$
$2_0^1 4_0^4$
4_0^6

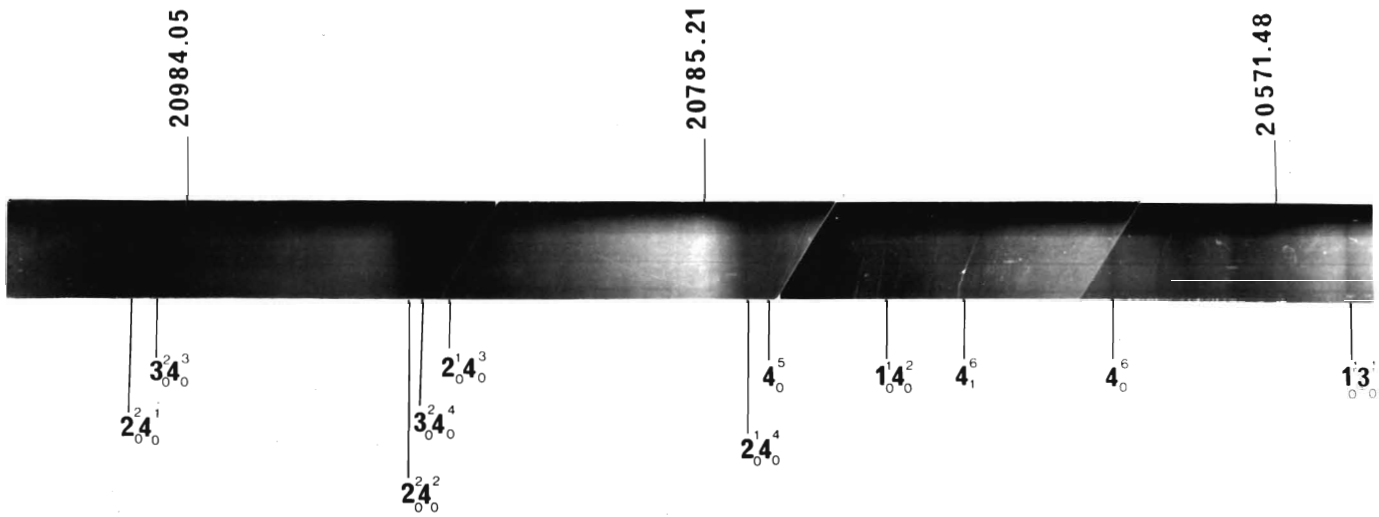
20984.05
20785.21
20571.48
$3^2_0 4^3_0$
$2^2_0 4^1_0$
$2^1_0 4^3_0$
$3^2_0 4^4_0$
$2^2_0 4^2_0$
4^5_0
$2^1_0 4^4_0$
$1^1_0 4^2_0$
4^6_1
4^6_0
$1^1_0 3^1_0$

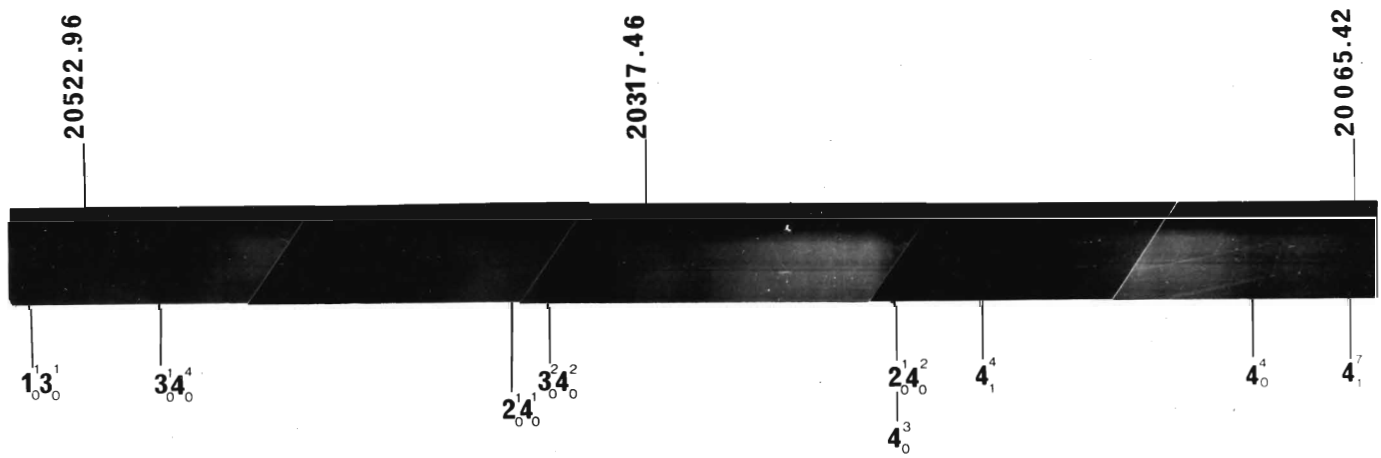
20522.96
20317.46
20065.42
$1^1_0 3^1_0$
$3^1_0 4^4_0$
$2^1_0 4^1_0$
$3^2_0 4^2_0$
$2^1_0 4^2_0$
4^3_0
4^4_1
4^4_0
4^7_1

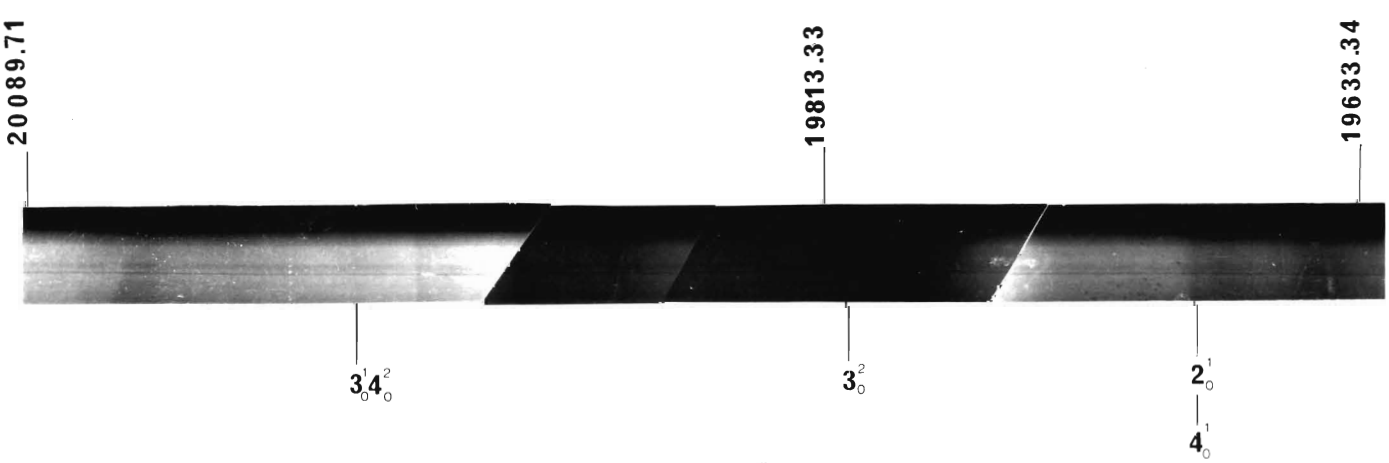
20089.71
19813.33
19633.34
$3^1_0 4^2_0$
3^2_0
2^1_0
4^1_0

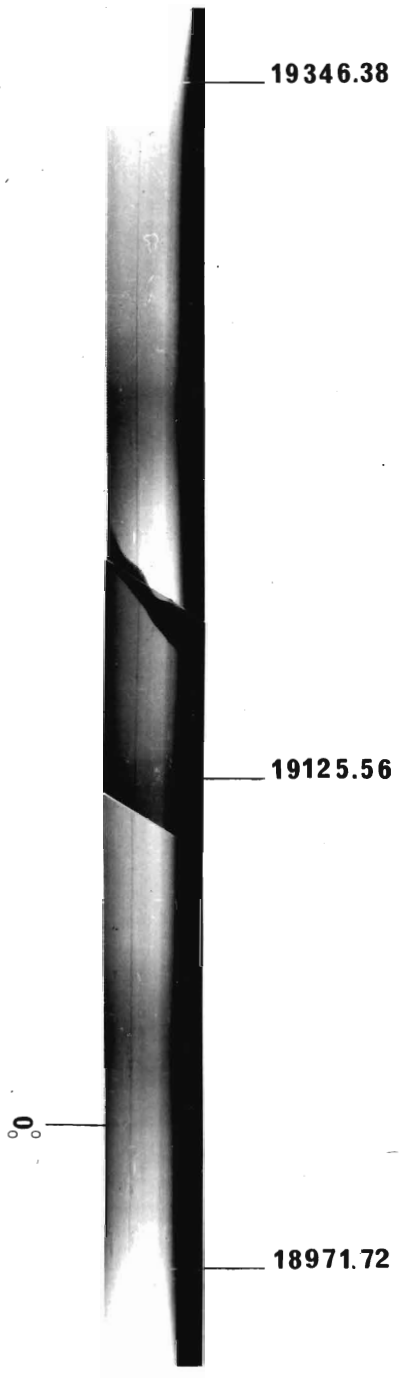
19346.38
19125.56
0_0^0
18971.72

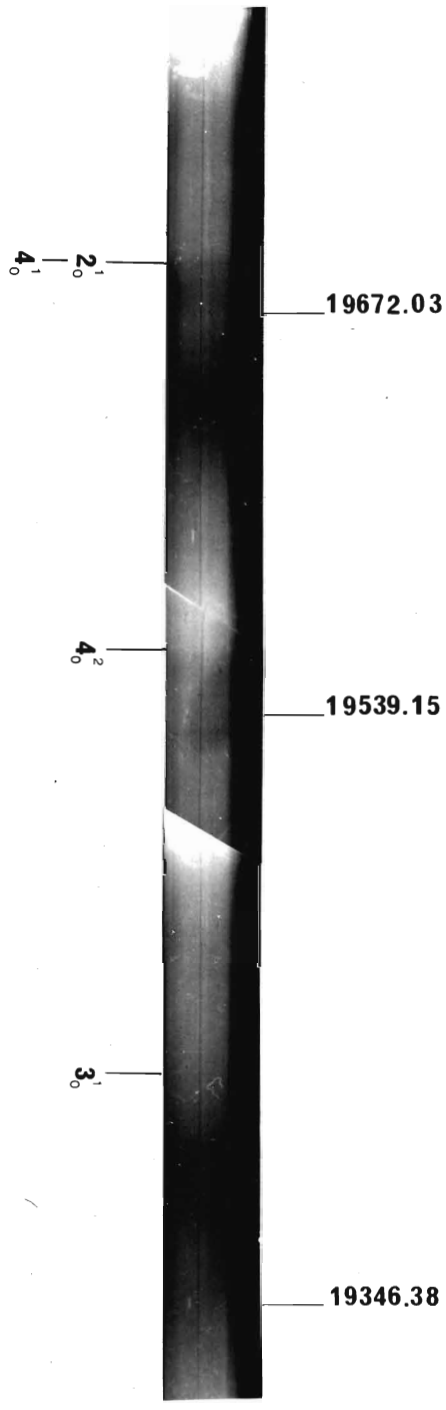
4_0^1 2_0^1
19672.03
4_0^2
19539.15
3_0^1
19346.38

FIGURE 9

(b) Microdensitometer Tracings of the Absorption Spectra of F_2CSe

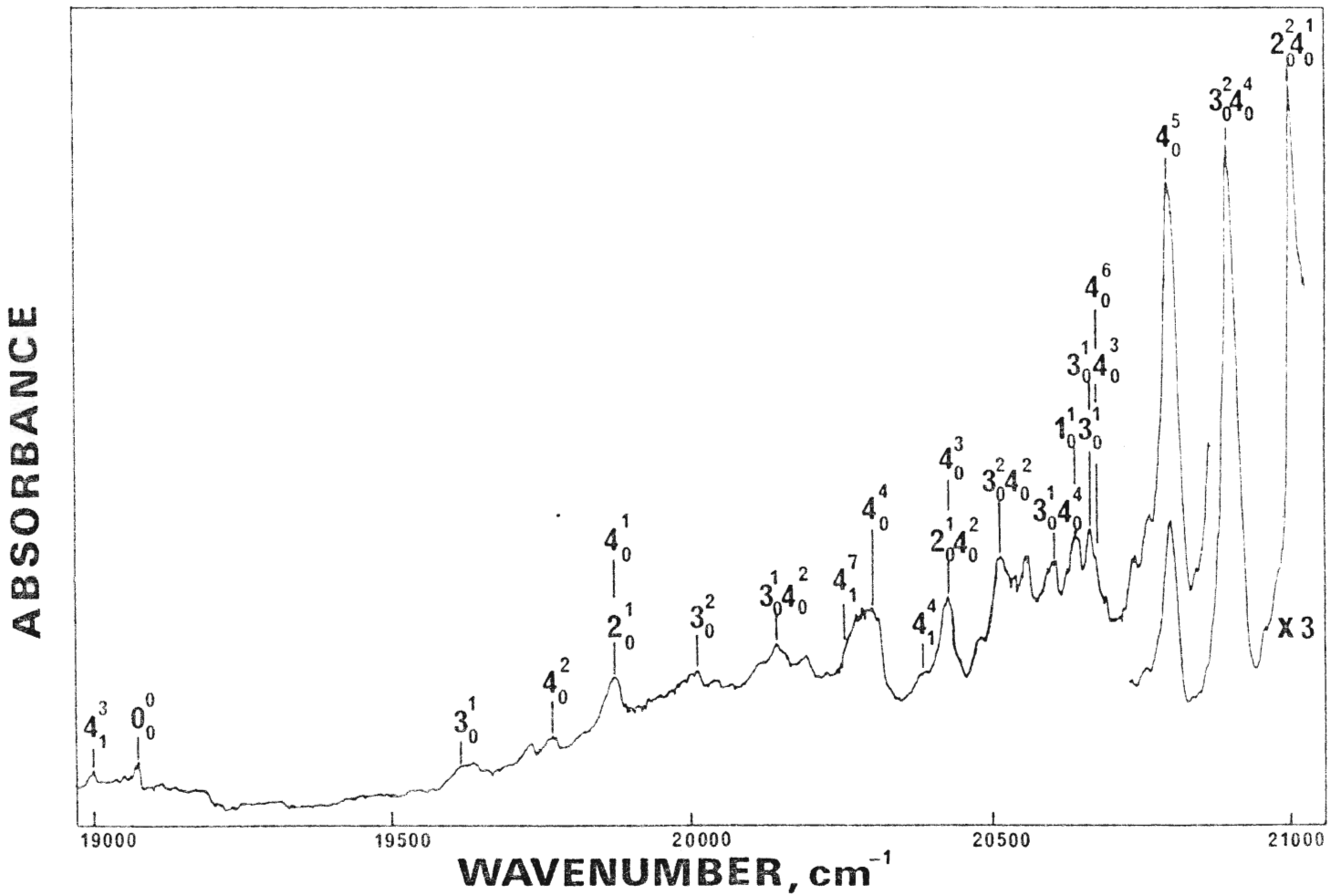
ABSORBANCE
WAVENUMBER, cm^{-1}
19000
19500
20000
20500
21000
4_1^3
0_0^0
3_0^1
4_0^2
2_0^1
4_0^1
3_0^2
$3_0^1 4_0^2$
4_1^7
4_0^4
4_1^4
$2_0^1 4_0^2$
4_0^3
$3_0^2 4_0^2$
$3_0^1 4_0^4$
$1_0^1 3_0^1$
$3_0^1 4_0^3$
4_0^6
4_0^5
$3_0^2 4_0^4$
$2_0^2 4_0^1$
X 3

TABLE 13

Band Frequencies and Assignments for the $\tilde{a}\ ^3A_2 \leftarrow \tilde{X}\ ^1A_1$ and $\tilde{A}\ ^1A_2 \leftarrow \tilde{X}\ ^1A_1$ Transitions in F_2CSe

Assignment	Band Type	Frequency (cm^{-1})
4_1^3	S-T	18986
0_0^0	S-T	19018
3_0^1	S-T	19415
4_0^2	S-T	19561
4_1^2	S-S	19653
2_0^1	S-T	19689
4_0^1	S-S	19689
3_0^2	S-T	19805
$3_0^1 4_0^2$	S-T	19953
4_1^7	S-T	20068
4_0^4	S-T	20103
4_1^4	S-S	20187
$2_0^1 4_1^5$	S-T	20198
$2_0^1 4_0^2$	S-T	20228
4_0^3	S-S	20228
$3_0^2 4_0^2$	S-T	20345
$2_0^1 4_0^1$	S-S	20351
$3_0^1 4_0^4$	S-T	20495
$1_0^1 3_0^1$	S-T	20545
$3_0^1 4_0^3$	S-S	20616
4_0^6	S-T	20633
4_1^6	S-S	20683
$1_0^1 4_0^2$	S-T	20717

Table 13 (cont'd.)

Assignment	Band Type	Frequency (cm^{-1})
4_0^5	S-S	20764
$2_0^1 4_0^4$	S-T	20770
$1_0^1 4_0^1$	S-S	20818
$2_0^1 4_0^3$	S-S	20886
$3_0^2 4_0^4$	S-T	20891
$2_0^2 4_0^2$	S-T	20896
$3_0^2 4_0^3$	S-S	20995
$2_0^2 4_0^1$	S-S	21007
$3_0^1 4_0^6$	S-T	21034
4_0^8	S-T	21128
$3_0^1 4_0^5$	S-S	21150
$1_0^1 2_0^1 3_0^1$	S-T	21201
$1_0^1 4_0^4$	S-T	21231
4_0^7	S-S	21284
$1_0^1 4_0^3$	S-S	21357
$2_0^2 3_0^1 4_0^1$	S-S	21393
$2_0^1 4_0^5$	S-S	21427
$1_0^1 3_0^2 4_0^2$	S-T	21490
$3_0^2 4_0^5$	S-S	21526
$2_0^2 4_0^3$	S-S	21545
$1_0^1 2_0^1 3_0^2$	S-T	21597
$2_0^3 4_0^1$	S-S	21662
$3_0^1 4_0^7$	S-S	21668
$1_0^1 2_0^1 3_0^2 4_0^1$	S-S	21718
4_0^9	S-S	21800

Table 13 (cont'd.)

Assignment	Band Type	Frequency (cm^{-1})
$2_0^2 3_0^1 4_0^3$	S-S	21926
$2_0^2 4_0^5$	S-S	22082
$2_0^3 4_0^3$	S-S	22200

TABLE 14

The Observed Energy Levels of the Out-of-Plane Mode ν_4' F_2CSe (cm^{-1})

ν_4'	$\tilde{a}\ ^3A_2$	$\tilde{A}\ ^1A_2$
0	0	0
1	0	0
2	543	539
3	543	539
4	1085	1073
5	1088	1075
6	1615	1569
7	1625	1595

It was found however that the addition of a quartic term in the potential function did not significantly improve the agreement between the observed and the calculated energy levels. Finally the Gaussian barrier term was replaced by a Lorentzian term. Satisfactory fits were obtained from this two-termed function for both excited states.

5.5.1 Harmonic Oscillator Perturbed by a Gaussian Term

The double-minimum potential created by superimposing a Gaussian and a harmonic oscillator potential has been constructed. Three independent parameters are required to specify the potential function. These have been related to the shape of the function by Coon, Naugle and McKenzie.[46]

The form of the potential function is

$$V(Q) = \frac{1}{2}\lambda Q^2 + A\exp(-a^2Q^2), \tag{5.1}$$

where Q is a mass adjusted coordinate defined by $2T = Q^2$, and λ, A, a^2 are three parameters. The Coon parameters ρ, ν_0, and B are defined by

$$\rho = \ln(2Aa^2/\lambda), \tag{5.2}$$

$$\nu_0 = \frac{\lambda^{\frac{1}{2}}}{2\pi c}, \tag{5.3}$$

$$B = \frac{2\pi}{h\lambda^{\frac{1}{2}}}\left[V(0) - V(Q_m)\right]. \tag{5.4}$$

ρ is a parameter determining the shape of the potential, ν_0 is the frequency of the parabolic part of the potential, and B is related to the height of the perturbing Gaussian barrier. For low values of ρ the outer walls of the potential rise more steeply than the walls of the barrier while the reverse effect is true for larger values of ρ.

The vibrational Hamiltonian for the inversion mode is written as

$$H = -\frac{h^2}{8\pi^2}\frac{d^2}{dQ^2} + \frac{\lambda}{2}Q^2 + A\exp(-a^2Q^2) \tag{5.5}$$

Regarding the last term as a perturbation, the Hamiltonian may be written as

$$H = H^o + H' \tag{5.6}$$

where

$$H' = A\exp(-a^2Q^2) \tag{5.7}$$

and H^o is the Hamiltonian of the harmonic oscillator.

The eigenvalues of H^o are

$$E_n = (n + \tfrac{1}{2})hc\nu_0 \tag{5.8}$$

and the normalized eigenfunctions are

$$X_n = N_n H_n(\alpha Q)\exp(-\alpha^2Q^2/2) \tag{5.9}$$

in which $H_n(\alpha Q)$ are the Hermite polynomials,

$$N_n = \left(\frac{\alpha}{\pi^{\frac{1}{2}}2^n n!}\right)^{\frac{1}{2}} \tag{5.10}$$

and

$$\alpha^2 = \frac{\lambda}{hc\nu_0} \tag{5.11}$$

The eigenfunctions of the vibrational Schrödinger equation can be approximated as

$$\phi_k = \sum_{n=0}^{N} c_{k2n}X_{2n} \tag{5.12}$$

for the symmetric levels and

$$\phi_j = \sum_{n=0}^{N} c_{j(2n+1)}X_{2n+1} \tag{5.13}$$

for the antisymmetric levels. The values of the coefficients of the eigen-

vectors and the eigen values of the Gaussian barrier-harmonic oscillator Hamiltonian operator are obtained by the linear variational theory[47] when the following secular equation is satisfied.

$$|H_{mn} - \delta_{mn}E| = 0 \tag{5.14}$$

where

$$H_{mn} = \int X_m(H^o + H')X_n dQ = \delta_{mn}E_n + H'_{mn} \tag{5.15}$$

and δ_{mn} is the Kronecker delta.

Since the Hamiltonian of equation (5.1) is dependent on the constants ρ, ν_0, and B, the eigenvalues obtained from the solution of the secular equation are dependent on the values chosen for these constants. The subroutines were available for calculating of the matrix elements and the diagonalization of the Hamiltonian matrix. The present calculations were carried out on a Burroughs 6700 computer, with 60 basis functions. Approximately 60 seconds of machine time were required to obtain the lowest eight energy levels.

The results obtained for the $\tilde{A}\ ^1A_2$ state with several different sets of parameters are presented in Table 15. Unfortunately, the residuals calculated from the analyses are disappointingly high. That is, the gap between the observed and experimental frequencies increase steadily as the vibrational quantum number increases.

5.5.2 Harmonic Oscillator Perturbed by a Gaussian and Quartic Terms

It was anticipated that the addition of a quartic term in the potential function would significantly improve agreement between the observed and the calculated levels. The new form of the potential function is

$$V(Q) = \frac{1}{2}\lambda Q^2 + A\exp(-a^2Q^2) + dQ^4 \tag{5.16}$$

TABLE 15

The Energy Levels of the $\tilde{A}\ ^1A_2$ State with Gaussian Barrier Type Functions

		$\rho = 1.50$		$\rho = 1.20$		$\rho = 0.26$	
		$B = 7.384$		$B = 5.917$		$B = 3.286$	
		$\nu_0 = 325.0\ cm^{-1}$		$\nu_0 = 365.0\ cm^{-1}$		$\nu_0 = 780.0\ cm^{-1}$	
ν_4'	Obs. (cm^{-1})	Calc.	Res.	Calc.	Res.	Calc.	Res.
0	0	0.00	0.00	0.00	0.00	0.00	0.00
1	0	0.00	0.00	0.00	0.00	0.00	0.00
2	539	539.87	-0.87	540.70	-1.70	537.20	1.80
3	539	539.89	-0.89	540.73	-1.73	537.20	1.80
4	1073	1053.86	19.14	1051.16	21.84	1047.66	25.34
5	1075	1054.29	20.71	1052.28	22.72	1047.66	27.34
6	1569	1533.02	35.98	1512.18	56.82	1524.86	44.14
7	1595	1539.46	55.54	1529.86	65.14	1525.28	69.72

A subroutine for the quartic contribution was added to the Gaussian-Quadratic program and vibrational energy levels were calculated. The results for the $\tilde{A}\ ^1A_2$ along with the results of similar calculations for the $\tilde{a}\ ^3A_2$ are presented in Table 16. By comparison of the results in Table 15 with those in Table 16 it is clear that the addition of the quartic term did not significantly improve the fit to the data.

5.5.3 Harmonic Oscillator Perturbed by a Lorentzian Term

The Gaussian barrier was replaced by a Lorentzian barrier in the one-dimensional double minimum problem. The new function is

$$V(Z) = AZ^2 + \frac{B}{c+Z^2} \ , \tag{5.17}$$

where Z is the reduced normal coordinate defined by Chan and Stelman[48] and is related to the displacement coordinate by

$$Z = (4\mu k/h^2)^{1/4}x \ . \tag{5.18}$$

In this equation k is the harmonic force constant, x the displacement coordinate, and μ the reduced mass. The matrix elements were set up using 60 harmonic oscillator wave functions as basis functions. The eigenvalues and eigenvectors were obtained by diagonalization of the resulting Hamiltonian.

It was found that the Lorentzian barrier perturbed harmonic oscillator gives energy level differences in good agreement with those observed for the $\tilde{A}\ ^1A_2$ and $\tilde{a}\ ^3A_2$ states. The best fit to the $\tilde{A}\ ^1A_2$ data was from the function

$$V(Z) = 81.4\ Z^2 + \frac{24500.00}{5.0 + Z^2} \ . \tag{5.19}$$

A similar fit to the $\tilde{a}\ ^3A_2$ data gave

$$V(Z) = 81.7\ Z^2 + \frac{29000.00}{5.2 + Z^2} \ . \tag{5.20}$$

TABLE 16

The Energy Levels for the $\tilde{A}\ ^1A_2$ and $\tilde{a}\ ^3A_2$ with Gaussian + Quartic Perturbed Functions

	$\tilde{A}\ ^1A_2$			$\tilde{a}\ ^3A_2$		
	$\rho = 1.52$			$\rho = 1.50$		
	$B = 7.8613$			$B = 7.384$		
	$\nu_0 = 318.0\ cm^{-1}$			$\nu_0 = 325.0\ cm^{-1}$		
	$d = 0.00060$			$d = 0.000261$		
ν_4'	Obs. (cm^{-1})	Calc.	Res.	Obs. (cm^{-1})	Calc.	Res.
0	0	0.00	0.00	0	0.00	0.00
1	0	0.00	0.00	0	0.00	0.00
2	539	540.40	-1.40	543	543.09	0.09
3	539	540.41	-1.41	543	543.10	0.10
4	1073	1056.58	16.42	1085	1060.04	24.96
5	1075	1056.85	18.15	1088	1060.52	27.48
6	1569	1540.97	28.13	1615	1541.07	73.93
7	1595	1545.31	49.69	1625	1548.32	76.68

Observed and calculated energy manifolds of ν_4' are shown in Table 17. The systematic increase in the residuals with the vibrational quantum number has been eliminated in this calculation. It would appear that for very high barriers the Lorentzian perturbed functions provide a superior fit to the data than do the Gaussian barriers.

5.6 Structural Analyses

The barriers in the double well functions of the $\tilde{A}\ ^1A_2$ and $\tilde{a}\ ^3A_2$ states were 2483 and 2923 cm^{-1}, respectively, while the corresponding values for Z_m, the minima in the functions, were 3.514 and 3.692, respectively. The relation between the mass adjusted coordinate and the reduced normal coordinate is

$$Q = \left(\frac{h}{4\pi\nu_0}\right)^{\frac{1}{2}} Z \ , \tag{5.21}$$

where Q is the mass adjusted coordinate and Z the reduced normal coordinate. As a result of this equation the minima points of $\tilde{A}\ ^1A_2$ and $\tilde{a}\ ^3A_2$ in the mass adjusted coordinate are $1.0304 \times 10^{-20}\ g^{\frac{1}{2}}cm$ and $1.0806 \times 10^{-20}\ g^{\frac{1}{2}}cm$.

The out-of-plane coordinate Q_4 is related to the angle displacement θ through the reduced mass relationship

$$Q_4(\theta) = \int_0^{\theta} \left[\mu(\theta)\right]^{\frac{1}{2}} r_{CSe}\, d\theta \ . \tag{5.22}$$

The variable reduced mass has been given by Jones and Coon[7] as

$$\mu(\theta) = \frac{2M_F l(m + l n \sin^2\theta)}{n(1-n) + 2lnR\cos\theta + l(1-l)R^2} \ .$$

Here $l = M_{Se}/M$, $m = M_C/M$, $n = 2M_F/M$.

$$M = M_{Se} + M_C + 2M_F \quad \text{and} \quad R = \frac{r_{CSe}}{r_{CF}\cos\beta} \ ,$$

TABLE 17

The Energy Levels of the Out-of-Plane Mode ν_4' F_2CSe (cm^{-1})

	$^1A_2$			$^3A_2$		
ν_4'	Obs.	Calc.	Res.	Obs.	Calc.	Res.
0	0	0.0	0.0	0	0.0	0.0
1	0	0.0	0.0	0	0.0	0.0
2	539	540.1	-1.1	543	548.7	-5.7
3	539	540.6	-1.6	543	548.7	-5.7
4	1073	1067.8	5.2	1085	1088.8	-3.8
5	1075	1072.1	2.9	1088	1090.1	-1.1
6	1569	1570.2	-1.2	1615	1614.5	0.5
7	1595	1594.7	0.3	1625	1622.4	2.6
8	-	2021.9		2110	2109.9	0.1
9	2111	2114.0	-3.0	-	2147.2	

where M_{Se}, M_C and M_F are the masses of selenium, carbon and fluorine atoms, r_{CSe} and r_{CF} are the CSe and CF bond lengths, and β is the FCF angle.

The model assumes that the normal coordinate Q_4 is derived from the internal coordinate θ which is defined as the angle between the CSe bond and the line bisecting the FCF angle. In this rigid model the β(FCF) angle and the CSe, CF bond lengths were kept constant.

For $\tilde{A}\ ^1A_2$ a value $\theta_m = 30.1^o$ and for $\tilde{a}\ ^3A_2$ a value $\theta_m = 31.4^o$ were obtained using $r_{CSe} = 1.743$ Å, $r_{CF} = 1.314$ Å and β(FCF) = 107.5^o ground state values.[23]

CHAPTER 6

DISCUSSION AND CONCLUSIONS

6.1 Correlation of the Electronic Energies

The $\pi^* \leftarrow n$ electronic excitation energies from the ultraviolet spectra have been combined with the values obtained from photoelectron spectra and have been used to obtain the energy levels of the three orbitals for the carbonyl, thiocarbonyl and selenocarbonyl compounds. The positions of the n and π orbitals were obtained from the photoelectron spectrum and Koopman's theorem.[3,7] This theorem states that orbital energy is equal to ionization energy. The level of the π^* orbitals was evaluated from the ultraviolet spectra by using the $\pi^* \leftarrow n$ excitation energy. The $\pi^* \leftarrow \pi$ excitation energy was not used because the singlet and triplet states have very different energies. The singlet-triplet gaps in the $\pi^* \leftarrow n$ transitions for the carbonyl and thiocarbonyl molecules are less than 3000 cm^{-1}. Certain trends can be observed when the energy levels are correlated between the different molecules. These are shown in Figure 10. The P.E.S. suggests that the n orbital is localized on the oxygen atom in H_2CO whereas in F_2CO the orbital extends over four atomic centers. Also, the n orbital is slightly more bonding in the oxygen containing molecules than in the analogous sulfur and selenium containing molecules. Selenium and sulfur atoms appear to have very similar properties. The $\pi^* \leftarrow n$ excitation of F_2CS[15] (2.91 ev) is very similar to that of F_2CSe (2.82 ev). The electronic spectrum suggests that the properties of F_2CSe should parallel those of F_2CS.

6.2 Barriers to the Molecular Inversion

The barrier heights for selenocarbonyl difluoride has been presented in Table 18 along with the values for the carbonyl and thiocarbonyl compounds for comparison purposes. There are large variations in the barrier heights

FIGURE 10

Correlation of the $\pi^* \leftarrow n$ Electronic Excitation Energy (ev) from the Ultraviolet Spectra with the Values Obtained from the Photoelectron Spectra

	H_2CO	Cl_2CO	F_2CO	H_2CS	Cl_2CS	ClFCS	F_2CS	F_2CSe
π^*	$(7.34)^{6}$	$(7.66)^{11}$	$(7.60)^{51}$	$(7.35)^{12}$	$(7.48)^{17}$	$(7.51)^{18}$	$(7.73)^{15}$	$(7.50)^{*}$
				9.38^{52}	9.80^{50}	10.20^{53}	10.64^{53}	10.32
n	10.88^{49}	11.83^{50}	13.60^{49}	11.76^{52}	10.88^{50}	11.20^{53}	11.71^{53}	
			14.60^{49}					
π	14.50^{49}							
		16.73^{50}						

*Expected value.

TABLE 18

Correlation of the Inversion Barriers (cm^{-1})

for the Substituted Tetra Atomic Carbonyl, Thiocarbonyl

and Selenocarbonyl Molecules

$\tilde{A}\ ^1A_2$

	O	S	Se
H	H_2CO[19] (316)	H_2CS[20] (0)	
Cl	Cl_2CO[11] (3170)	Cl_2CS[17] (598)	
F	F_2CO[10] (8200)	F_2CS[15] (3076)	F_2CSe (2483)

$\tilde{a}\ ^3A_2$

	O	S	Se
H	H_2CO[19] (762)	H_2CS[20] (7)	
Cl	Cl_2CO (-)	Cl_2CS[17] (726)	
F	F_2CO (-)	F_2CS[40] (>3100)	F_2CSe (2923)

to molecular inversion. The inversion barrier is sensitive to the type of substituent of either ends of the molecules. Another point is that the triplet state of these molecules have higher barrier heights than they have in the singlet state.

To obtain an insight into the factors responsible for the variation in barrier with change in substituent, Walsh's rule has been extended to chlorine and fluorine substituted compounds. The main principle on which the correlation has been based is that: an orbital becomes more tightly bound as the s density increases on that atom. The degree of non-planarity in the $\tilde{a}$ and $\tilde{A}$ states depends upon the amount of s character acquired by the π^* orbital. The height of the inversion barrier should then parallel the $2p_x$ and 2s density changes at the carbon atom. The effect of substitution of electronegative halogens for hydrogen has a stabilizing effect on the σ MO's but not on the π MO's. This effect has been observed on a photoelectron study of F_2CO and H_2CO by Brundle et al.[49] Therefore the $2p_x$(C) AO which goes to form the π MO is relatively unaffected by substitution on the carbonyl group. The σ MO's in these compounds belong to the a_1 and b_2 species, while the π and π^* MO's belong to the b_1 representation. When the molecule is distorted from the planar C_{2v} symmetry to the nonplanar C_s form, the a_1 and b_1 species correlate with a', and the a_2 and b_2 correlate with a" of the C_s point group. Therefore in a nonplanar system, the σ - π distinction is no longer valid. It follows that the electron density is pulled from the O, S or Se atoms to the C atom by an electronegative substituent. The carbon $2p_x$ AO responds to halogen induction effects with the result that there is a net charge flow from the $2p_x$(C) into the 2s(C) AO. From the view point of the Walsh postulate, a change in electron density in this direction would result in a nonplanar distortion at the carbon center. In the series of halogen substituents,

fluorine has a greater electronegativity than chlorine. Therefore fluorine substituents have a higher barrier than chlorine substituents. For example the inversion barrier for H_2CO, Cl_2CO and F_2CO are 316, 3170 and 8200 cm^{-1} respectively in the $\tilde{A}\ ^1A_2$ state.

The barrier height decrease from the carbonyl compound to the seleno-carbonyl compound is expected according to Walsh's rules. The selenium atomic orbitals are larger and more diffuse than sulfur orbitals. Therefore during the electron promotion, the density flow from the sulfur atom to the carbon atom is greater than the corresponding flow from the selenium atom. The barrier height change from 2483 cm^{-1} for F_2CSe to 3076 cm^{-1} for F_2CS is not unreasonable.

As it is shown in Table 18, the triplet state for each compound has a higher barrier than the singlet state. In the triplet state the single electrons in the n and π^* orbitals avoid each other through Pauli repulsion forces and additional density is pushed onto the carbon atom. This additional density at the carbon atom will distort the molecule even further from the planar configuration. The barrier heights for the singlet and triplet states of F_2CSe are found to be comparable with each other and with the other molecules in this series.

6.3 The Excited State Fundamentals

F_2CSe frequencies in the $\tilde{X}$, $\tilde{A}$ and $\tilde{a}$ states are shown in Table 19 along with the frequencies of F_2CS and F_2CO. The excited state set of frequencies are not complete, and a normal coordinate analysis to investigate the upper state vibrational dynamics is not possible.

It appears to be a general phenomenon that the C═Se and C═S stretching frequencies are higher in the $\tilde{a}$ state than they are in the $\tilde{A}$ state. G. W. Robinson[54] observed this effect for H_2CO and he predicted that the differences

TABLE 19

Vibrational Frequencies (cm^{-1}) of F_2CSe, F_2CS and F_2CO in the Ground and First Excited States

	F_2CSe			F_2CS			F_2CO	
	$\tilde{X}^{22}$	$\tilde{A}$	$\tilde{a}$	$\tilde{X}^{30}$	$\tilde{A}^{11}$	$\tilde{a}^{40}$	$\tilde{X}^{29}$	$\tilde{A}^{10}$
$\nu_1(a_1)$	1287	1129	1156	1365.2	1100.6	1186	1929.9	1030
$\nu_2(a_2)$	705	662	671	789.3	736.5	729	965.6	830
$\nu_3(a_1)$	432	388	397	526.2	385.8	391	582.9	465
$\nu_4(b_1)$	575	539	543	623.2	557.9	566	767.4	670
$\nu_5(b_2)$	1207	-	-	1200	-	-	1243.7	1216
$\nu_6(b_2)$	351	-	-	418	-	-	619.9	-

in frequencies in the two electronic states could be used to distinguish bands of the singlet-triplet system from those of the singlet-singlet system.

The three totally symmetric (a_1) vibrations of F_2CO in the $\tilde{X}$ state are well separated from each other and may be designated valence vibrations. The 1929.9 cm^{-1} frequency can be assigned to the ν_1 C═O stretching mode while the 965.6 cm^{-1} to the C—F stretching mode and 582.9 cm^{-1} to the FCF angle bending mode. Without the complications of the internal coordinate mixing the ν_1 mode should decrease uniformly in the thiocarbonyl and selenocarbonyl compounds while ν_2 should remain constant. The reduction from 965.6 cm^{-1} to 789.3 cm^{-1} and to 705 cm^{-1} must be an indication of an increasing mixing between the ν_1 and ν_2 modes as the mass at the end of the molecule increases. This approach is true for the FCF angle bending mode as well. The frequency drops uniformly from 582.9 cm^{-1} to 526.2 cm^{-1} and to 432 cm^{-1}.

This simple relationship does not appear to hold among the ν_1, ν_2 and ν_3 frequencies in the $\tilde{A}$ excited states of the three substituted fluorine compounds. For example ν_1 appears to be anomalous. F_2CO has a frequency of 1030 cm^{-1} which climbs to 1100.6 cm^{-1} in F_2CS and then to 1129 cm^{-1} in F_2CSe. That is, the frequency increases with the mass of the substituent. On the other hand ν_2 decreases with the increasing of the mass of substituent from 830 cm^{-1} to 736.5 cm^{-1} to 662 cm^{-1}. This ordering is parallel to the trend in the ground state. ν_3 drops from 465 cm^{-1} to 385 cm^{-1} and then climbs to 388 cm^{-1} in the three molecules respectively.

The behaviour in ν_1 can be explained in terms of the ratios of the frequency drop on excitation $\tilde{A}/\tilde{X}$ in the three fluorine substituted molecules. They are for F_2CO: 1030/1929.9; for F_2CS: 1100.6/1365.2; and for F_2CSe: 1129/1287. The reduction in frequency then is greatest for carbonyl compounds followed by the thio and selenocarbonyl compounds. If ν_1 is assumed to be a

valence vibration in the $\tilde{X}$ and $\tilde{A}$ states it is possible to predict the change in bond length on excitation through use of the empirical rule ωr^3 = constant.[55] With this empirical rule $\Delta r(r' - r'')$ for the $\tilde{A}$ and $\tilde{X}$ states are 0.272 Å, 0.118 Å and 0.077 Å for the C=O, C=S and C=Se bonds respectively. The change in the C=O, C=S and C=Se bond lengths can be considered in terms of the $\pi^* \leftarrow$ n electron promotion. Information about the removal of the nonbonding electron comes from the photoelectron spectra. In F_2CS the 1365.2 cm^{-1} values of the ν_1 mode of the $\tilde{X}$ state increases to 1370 cm^{-1} [53] whereas the 1929.9 cm^{-1} value in F_2CO drops to 1550 cm^{-1} [49] on ionization. That is, the loss of the electron in the thiocarbonyl molecule decreases the C=S bond length very slightly whereas the same ionization process in F_2CO increases the C=O bond length. The C=S bond length decrease (Δr) is 0.002 Å and the C=O bond length increase is 0.088 Å. The conclusion follows that the nonbonding n orbital is slightly antibonding in F_2CS whereas in F_2CO it is strongly bonding. The n orbital is shifted relative to the bonding energy of the π orbital for F_2CO as it is shown in Figure 10.

The conclusion that can be drawn from these correlations is that the change in ν_1 frequency on excitation from $\tilde{X}$ state to $\tilde{A}$ state is sensitive less to the loss of the n electron than it is to the introduction of the electron into the π^* orbital. In the case of F_2CO the introduction of the π electron destabilizes the C=O bond length by 0.184 Å. The same destabilization in thiocarbonyl difluoride is 0.120 Å. These results are not unexpected and it is reasonable that the π^* orbital in F_2CS should be slightly less antibonding than it is in F_2CO. Without the photoelectron spectrum for F_2CSe these rough correlations can not be given. It would be anticipated that the bond length changes should parallel those of F_2CS.

6.4 Singlet-Triplet Splitting

The correlation of the singlet-triplet intervals among the carbonyl, thiocarbonyl and selenocarbonyl molecules are also of interest. The singlet-triplet splitting for $\pi^* \leftarrow$ n electron promotion is 3000 cm^{-1} in H_2CO.[7] This gap falls to 1887 cm^{-1} in H_2CS,[14] 1224 cm^{-1} in Cl_2CS[56] and 671 cm^{-1} in F_2CSe.

In a triplet state an unpaired electron repels another unpaired electron of the same spin and forces the electron density of the two electrons to have low amplitudes in the region when they are near each other. This is known as the Fermi Hole which takes the form of a region around each electron where no other electron with the same spin is likely to be. Fermi correlation effects which cause the singlet-triplet gap are expected to be large in a narrow space and small in a big space.[57]

The singlet-triplet gap values of H_2CO and its prototypes depend on how far the n unpaired electron is from the π^* unpaired electron which has the same spin. Therefore different gap values are attributed to the differences in their π^* and n orbital densities and the electronegativity of the halogen substituent. The diffuseness of these orbitals increases from carbonyl through thiocarbonyl to selenocarbonyl compounds. F_2CSe has large and diffuse molecular orbitals on the selenium atom which provide space for the two unpaired parallel spin electrons. Fermi correlation effects are expected to be smaller for F_2CSe than they are in the other prototypes. The 671 cm^{-1} singlet-triplet splitting observed here and the order of the splittings of H_2CO, H_2CS, Cl_2CS and F_2CSe are in accord with the concept of the Fermi Correlation Hole.

6.5 Conclusions

At some time in the future the spectroscopy of the selenocarbonyl compounds will be explored in detail and a complete correlation carried out among the various selenocarbonyl halide molecules.

This work represents the first example of such a spectral correlation. The major conclusion which was obtained in this study is that the properties of F_2CSe can be obtained by an extrapolation of the properties of the sulfur and the oxygen analogs. That is, to a good approximation, one can hold the low resolution spectrum of F_2CSe against the spectrum of F_2CS and observe a one-to-one correlation in the positions and intensities of the bands. The oxygen containing molecule however is shifted sufficiently in frequency that correlations become more difficult. For example the $\pi^* \leftarrow \pi$ transition in F_2CO has not been authenticated in the spectrum. However transitions in the vacuum UV[9] at 140 nm have been given this assignment. In H_2CO the $\pi^* \leftarrow \pi$ transition has not been observed directly. It is believed that the system autoionizes before the $\pi\pi^*$ state is reached.

One of the major difficulties which impedes the progress in the spectroscopy of the selenocarbonyl molecules is their extreme toxicity. The result is that the experiments have to be carried in a sealed vacuum system which at the end of the experiments must be destroyed. These experiments were completed in the course of four days. Further work to explore the vacuum spectrum of this molecule is not contemplated for this reason.

The H_2CSe molecule represents the prototype species in this series of molecules. For this reason and because it is expected to have a very open spectrum, it is the subject of some interest. An attempt was made to record the spectrum of H_2CSe using the same route which has proved to be so useful in the production of H_2CS. Trimethylene selenide was synthesized and passed through a pyrolysis tube at a series of temperatures before being admitted to an absorption cell. Unfortunately the observed spectrum did not have the $\pi^* \leftarrow \pi$ or $3s \leftarrow n$ absorption bands expected for H_2CSe. Again the toxicity of this system forced us to abandon this project. It is our belief that flash

photolysis could prove to be a more fruitful way of producing the seleno-carbonyl prototype.

REFERENCES

1. C. M. L. Kerr and D. A. Ramsay, J. Mol. Spec., 87, 575 (1981).

2. A. D. Walsh, J. Chem. Soc., 2306 (1953).

3. J. C. D. Brand, J. Chem. Soc., 858 (1956).

4. D. C. Moule and A. D. Walsh, Chem. Rev., 75, 67 (1975).

5. V. A. Job, V. Sethuraman and K. K. Innes, J. Mol. Spec., 30, 365 (1969).

6. V. Sethuraman, V. A. Job and K. K. Innes, J. Mol. Spec., 33, 189 (1970).

7. V. T. Jones and J. B. Coon, J. Mol. Spec., 31, 137 (1969).

8. G. Fischer, J. Mol. Spec., 29, 37 (1969).

9. G. L. Workman and A. B. F. Duncan, J. Chem. Phys., 52, 3204 (1970).

10. D. C. Moule, J. Chem. Phys. (in press).

11. D. C. Moule and P. D. Foo, J. Chem. Phys., 55, 1262 (1971).

12. R. H. Judge and G. W. King, J. Mol. Spec., 74, 175 (1979).

13. R. H. Judge and G. W. King, J. Mol. Spec., 78, 51 (1979).

14. R. H. Judge, D. C. Moule and G. W. King, J. Mol. Spec., 81, 37 (1980).

15. D. C. Moule and A. K. Mehra, J. Mol. Spec., 35, 137 (1970).

16. J. C. D. Brand, J. H. Colloman, D. C. Moule, J. Tyrell and T. H. Goodwin, Trans. Faraday Soc., 61, 2365 (1965).

17. D. C. Moule and C. R. Subramaniam, J. Mol. Spec., 48, 336 (1973).

18. C. R. Subramaniam and D. C. Moule, J. Mol. Spec., 53, 443 (1974).

19. P. Jensen and P. R. Bunker, J. Mol. Spec. (in press).

20. P. Jensen and P. R. Bunker, J. Mol. Spec. (in press).

21. A. Haas, H. Willner, H. Bürger and G. Pawelke, Spectrochimica Acta, 33A, 937 (1977).

22. A. Haas, B. Koch, N. Welcman and H. Willner, Spectrochimica Acta, 32A, 497 (1976).

23. D. Christen, H. Oberhammer, W. Zeil, A. Haas and A. Darmadi, J. Mol. Structure, 66, 203 (1980).

24. D. G. Carroll, L. G. Vanquickenborne and S. P. McGlynn, J. Chem. Phys., 45, 2777 (1966).

25. R. J. Buenker and S. D. Peyerimhoff, J. Chem. Phys., 53, 1368 (1970).

26. N. C. Baird and J. R. Swenson, J. Phys. Chem., 77, 277 (1973).

27. P. J. Bruna, S. D. Peyerimhoff, R. J. Buenker and P. Rasmus, Chem. Phys., 3, 35 (1974).

28. F. A. Cotton, "Chemical Applications of Group Theory", Wiley-Interscience, New York (1963).

29. P. D. Mallison, D. C. McKean, J. H. Holloway and I. A. Oxton, Spectrochimica Acta, 31A, 143 (1975).

30. A. J. Downs, Spectrochimica Acta, 19, 1165 (1963).

31. G. Herzberg, "Infrared and Raman Spectra of Polyatomic Molecules", D. Van Nostrand Reinhold Company, New York (1945).

32. M. J. Hopper, J. W. Russell and J. Overend, Spectrochimica Acta, 28A, 1215 (1972).

33. G. W. King, "Spectroscopy and Molecular Structure", Holt, Rinehart and Winston Inc., New York (1964).

34. G. Herzberg and E. Teller, Z. Physik. Chem., B21, 410 (1933).

35. J. A. Pople and J. W. Sidman, J. Chem. Phys., 27, 1270 (1957).

36. D. S. McClure, J. Chem. Phys., 20, 682 (1952).

37. M. Orchin and H. H. Jaffé, "Symmetry, Orbitals and Spectra", Wiley-Interscience, New York (1971).

38. D. C. Moule, F. D. Foo and A. Biernacki, J. Phys. Ed., 4, 449 (1971).

39. H. M. Crosswhite, "The Iron-Neon Hollow Cathode Spectrum", Journal of Research of the National Bureau of Standards - A Physics and Chemistry, Vol. 79A, No. 1, 17 (1975).

40. D. C. Moule, Can. J. Chem., 48, 2623 (1970).

41. J. E. Wollrab, "Rotational Spectra and Molecular Structure", Academic Press, New York (1967).

42. G. W. Rathgens, N. K. Freeman, W. D. Gwinn and K. S. Pitzer, J. Am. Chem. Soc., 75, 5634 (1953).

43. N. W. Naugle, J. R. Henderson and J. B. Coon, Symposium on Molecular Structure and Spectroscopy, The Ohio State University, June 1953; Bull. Am. Phys. Soc. 2 , 4, 105 (1959).

44. S. I. Chan, J. Zinn, J. Fernandez and W. D. Gwinn, J. Chem. Phys., 33, 1643 (1960).

45. J. D. Swalen and J. A. Ibers, J. Chem. Phys., 36, 1914 (1962).

46. J. B. Coon, N. W. Naugle and R. D. McKenzie, J. Mol. Spec., 20, 107 (1966).

47. I. N. Levine, "Quantum Chemistry", Allyn and Bacon, Boston (1977).

48. S. L. Chan and D. Stelman, J. Mol. Spec., 10, 278 (1963).

49. C. R. Brundle, M. B. Robin, N. A. Kuebler, and H. Basch, J. Am. Chem. Soc., 94, 1451 (1972).

50. D. Chadwick, Can. J. Chem., 50, 737 (1972).

51. E. R. Farnworth, G. W. King and D. C. Moule, Chem. Phys., 1, 82 (1973).

52. B. Soluoki, P. Rasmus and H. Bock, J. Am. Chem. Soc., 98, 6054 (1976).

53. K. Wittel, A. Haas and H. Bock, Chem. Ber., 105, 3865 (1972).

54. V. E. DiGiorgio and G. R. Robinson, J. Chem. Phys., 31, 1678 (1959).

55. C. H. D. Clark, Phys. Rev., 47, 238 (1935).

56. D. J. Clouthier and D. C. Moule, J. Mol. Spec., 87, 471 (1981).

57. S. P. McGlynn, T. Azumi and M. Kinoshita, "Molecular Spectroscopy of the Triplet State", Prentice Hall, New Jersey (1969).